The Pennsylvania State University

The Graduate School

Department of Geosciences

INVESTIGATING THE PALEOCENE-EOCENE CARBON-CYCLE PERTURBATION:

AN EARTH SYSTEM MODEL APPROACH

A Thesis in

Geosciences

by

Karla Michelle Panchuk

Submitted in Partial Fulfillment
of the Requirements
for the Degree of

Doctor of Philosophy

August 2007

The thesis of Karla Michelle Panchuk was reviewed and approved* by the following:

Lee Kump
Professor of Geosciences
Thesis Advisor
Chair of Committee

Klaus Keller
Assistant Professor of Geosciences

Raymond Najjar
Associate Professor of Meteorology

Timothy Bralower
Professor of Geosciences
Head of the Department of Geosciences

*Signatures are on file in the Graduate School

ABSTRACT

The Paleocene-Eocene Thermal Maximum, or PETM, was a time of sudden and major environmental change 55 million years ago, linked to a ~200 ka interval of global warming. It has been difficult to identify the cause of the PETM, however, because the <10 ka onset of the event is too rapid to explain by processes that operate on geologic timescales. This project was directed at using changes in the marine record of the PETM, a negative $\delta^{13}C$ excursion, and a decrease in $CaCO_3$ wt%, along with an Earth system model to better understand the cause and characteristics of the PETM.

A two-fold approach is presented here that utilizes the capabilities of the GENIE-1 Earth system model to simulate the spatial distribution of $CaCO_3$ on the sea floor, and to generate synthetic sediment cores. Chapter 2 presents a comparison of simulated patterns of sea floor $CaCO_3$ distribution with the observed PETM distribution of $CaCO_3$. Pulses of CO_2 ranging from 2,300 Pg C to 70,000 Pg C were added to the model Late Paleocene Earth system to simulate the isotopic end-members of potential sources, biogenic methane ($\delta^{13}C$ of -60‰) and mantle CO_2 ($\delta^{13}C$ of -5‰). A pulse of 7,000 Pg C came closest to reproducing observations when variable rates of sediment mixing by bioturbation were permitted.

In Chapter 3 the $\delta^{13}C$ and sediment records generated from these simulations were analysed to determine what processes affect the final $\delta^{13}C$ excursion that is recorded in sediments, and how well this excursion refects the $\delta^{13}C$ of surface ocean DIC. Key

factors determining the magitude of the $\delta^{13}C$ excursion recorded in sediments are the rate of recovery of the saturation state of seawater, and sediment mixing by bioturbation.

TABLE OF CONTENTS

LIST OF FIGURES

LIST OF TABLES

ACKNOWLEDGEMENTS

I knew I was in trouble when they stopped using numbers.
-Anonymous mathphobe

Sincere thanks go to:

Lee Kump
for invaluable advice and insight, patience, and for disagreeing frequently and energetically;

Klaus Keller
for mentorship, friendship, and calling it as he sees it;

Andy Ridgwell
for giving of his time and expertise with seemingly infinite generosity (though he should really take more vacations);

Tim Bralower and Ray Najjar
for a thorough reading of the manuscript and detailed annotations

Matt, Katja, Burt, Chris, Lisa, Geoff, Tyrone, and Scott
for friendship, thoughtful conversations, and pleasant coffee breaks;

Pearl, Irene, and Niels
for taking good care of me;

and Jeff
for gleefully finding my spelling mistakes, and patiently waiting for me to not be a student anymore.

Chapter 1

Overview

The Paleocene-Eocene boundary interval was a time of sudden and major environmental change 55 million years ago, linked to a short interval (~200 ka, Rohl et al., 2000) of global warming, referred to as the Paleocene-Eocene Thermal Maximum, or PETM. Evidence of PETM warming in the rock record is accompanied by carbon isotope excursions (CIEs) of -2.5 to -4‰ in the marine realm (e.g., Kennett and Stott, 1991; Cramer et al., 1999; Zachos et al., 2003; Fig. 1-1), and -5 to -7‰ in the terrestrial realm (e.g., Bowen et al., 2004 and references therein), suggesting that the warming was caused by a pulse of carbon input with a low carbon isotope composition ($\delta^{13}C$). This is consistent with another feature of the PETM, widespread dissolution of $CaCO_3$ in marine sediments (e.g., Zachos et al., 2005; Murphy et al., 2006; Fig. 1-1).

The PETM has generated much interest for two main reasons: First, it is viewed as an analogue of the kind of climate change event that is being driven by anthropogenic emissions of greenhouse gasses. Second, it has defied explanation by the usual means. Often, negative $\delta^{13}C$ excursions can be explained by the transfer of carbon from organic to inorganic sedimentary carbon reservoirs (e.g., an increase in weathering of fossil organic matter on land and its ultimate remineralization to dissolved inorganic carbon in seawater). At the PETM, however, the onset of the $\delta^{13}C$ excursion was rapid, perhaps even less than 10 ka (e.g., Kennett and Stott, 1991), an unreasonably short period of time to transfer the large amount of carbon required to generate such a large and global $\delta^{13}C$

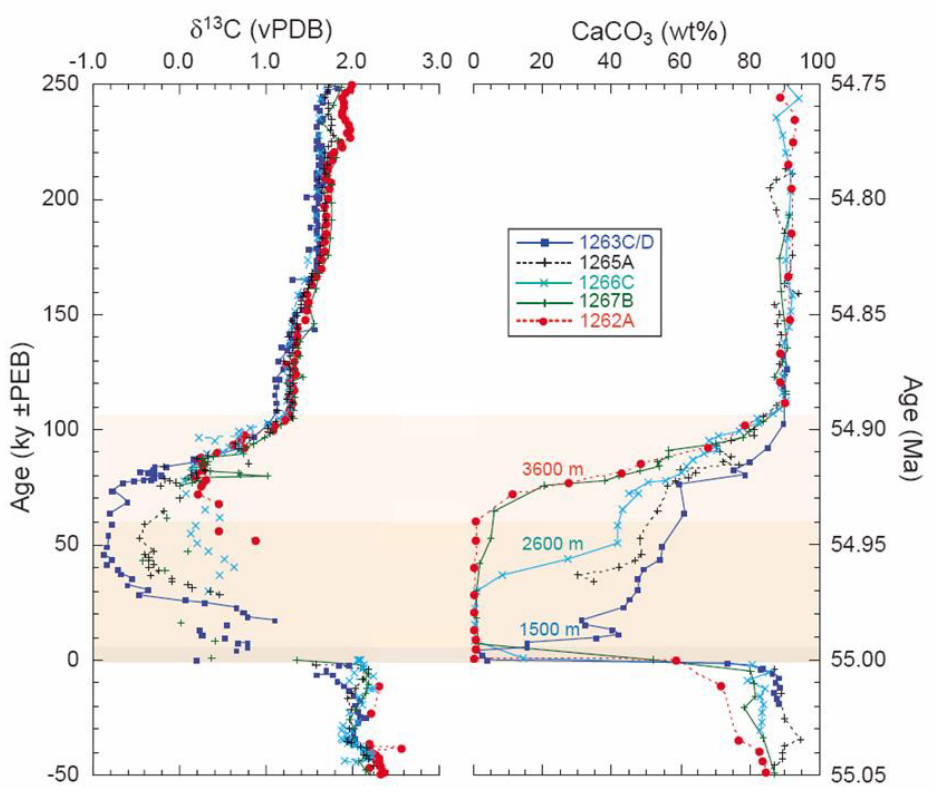

Figure 1-1: PETM $\delta^{13}C$ and $CaCO_3$ wt% records from Walvis Ridge in the southern Atlantic Ocean. Dark, medium, and light shading represent the onset, body, and recovery of the event, respectively. From Zachos et al. (2005).

perturbation through slow geological mechanisms. Dickens et al. (1995) framed the problem thus: to generate a -3‰ $\delta^{13}C$ excursion in the modern ocean and atmospheric carbon reservoir over 10 ka, mass balance calculations indicate that more organic carbon ($\delta^{13}C$ ~-25‰) would have to be buried in the ocean than presently exists in the terrestrial carbon reservoir. Furthermore, if the excursion were to be generated by volcanic degassing of mantle CO_2 ($\delta^{13}C$ ~-5‰), degassing would have had to occur at a rate 125 times greater than estimated long-term rates. The only reasonable alternative, these authors suggested, was that the carbon came from biogenic methane ($\delta^{13}C$ ~-60‰) and

that the methane was derived from thermal dissociation of methane clathrates within marine sediments. Other sources of carbon have been suggested since then, including organic carbon, both terrestrial from the burning of massive Upper Paleocene peat deposits (Kurtz et al., 2003), and marine, from desiccated epeiric sea sediments (Higgins and Schrag, 2006); thermogenic methane generated by sill emplacement within organic-rich sediments during North Atlantic Igneous Province volcanism (Svensen et al., 2004; Storey et al., 2007); and even extraterrestrial carbon from cometary impact (Kent et al., 2003).

Mass balance arguments can be used to determine how much carbon from a particular source is required to generate the CIE, but mass balance cannot provide a unique solution. There are many possible combinations of $\delta^{13}C$ and carbon flux magnitudes that could generate the observed $\delta^{13}C$ excursion, especially if multiple sources are considered. Further constraints are required to narrow down the options. This project was directed at using the observed $CaCO_3$ wt% distribution from below and within the PETM interval to guide an Earth system model configured for the Late Paleocene.

The tool used for this study is the Earth system model GENIE-1 (Grid ENabled Integrated Earth system model). The version of GENIE-1 used here (Lenton et al., 2006) comprises the coupled ocean-atmosphere model C-GOLDSTEIN (Edwards and Marsh, 2005 and references therein), a model of marine biogeochemical cycling (Ridgwell, 2001; Ridgwell et al., 2007), and a sediment model that can predict the $CaCO_3$ content of sea floor (coretop) sediments, has the option to simulate bioturbation, and can generate a

synthetic sediment column for direct comparison with marine cores (Ridgwell and Hargreaves, 2007).

There were several advantages to GENIE-1 over other models that led to its use for this project. GENIE-1 is a fully 3-D ocean model, but because of simplified frictional geostrophic physics and a relatively coarse resolution it runs orders of magnitude faster than other models initially considered for this study, including the Bern 2.5D model and an EMIC to be built in-house with the Geophysical Fluid Dynamic Lab's Modular Ocean Model 3 (MOM3) at its core. GENIE-1 also has great flexibility with respect to computing platforms. A further advantage of GENIE-1 was the coincidence of objectives between this study, and the developers of the coupled ocean-atmosphere component of GENIE-1, C-GOLDSTEIN, at the National Oceanographic Center in Southampton, UK. These researchers were interested in pursuing simulations with paleogeographic reconstructions, and were looking specifically at the ocean circulation at the Paleocene-Eocene boundary. As a result of using GENIE-1, this project also benefited enormously from the assistance of Andrew Ridgwell, who was developing the marine biogeochemical and sediment chemistry portions of the model along the lines of his Ph.D. thesis model, SUE (Ridgwell, 2001) at the beginning of our collaboration. Andrew Ridgwell worked on upgrades to the model throughout the course of the study, including development of synthetic model sediment cores. This capability allows a far more direct comparison between model results and data, it is certain to provide valuable insights into how diagenetic processes are recorded in sea floor sediment cores.

The outcome of this project is two manuscripts. The first manuscript presents a comparison of observed PETM $CaCO_3$ wt% with model core top $CaCO_3$ wt% values for

eight carbon release scenarios. Carbon release scenarios were selected to span the range of $\delta^{13}C$ of possible carbon sources. The low $\delta^{13}C$ end-member is biogenic methane ($\delta^{13}C$ of -60‰), and the high $\delta^{13}C$ end-member is mantle CO_2 ($\delta^{13}C$ of -5‰). Intermediate scenarios include $\delta^{13}C$ of -22‰, representative of organic carbon from peat (Kurtz et al., 2003), and $\delta^{13}C$ of -12, -9.5, and -6‰, reflecting combinations of high $\delta^{13}C$ carbon derived from mantle CO_2 and low $\delta^{13}C$ carbon as from biogenic methane, organic carbon, or thermogenic methane ($\delta^{13}C$ of -35 to -50‰, Hunt, 1996). Although the average PETM CIE has been cited as -2.5 to -3‰ (e.g., Dickens et al., 1995; Pagani et al., 2006), a survey of published $\delta^{13}C$ analyses conducted for this project suggests that an excursion of -4‰ is more appropriate. The requisite carbon pulses for carbon sources with $\delta^{13}C$ of -60, -22, -12, -9.5, -6, and -5‰ are 2,300, 7,000, 15,000, 21,000, 46,000, and 70,000 Pg C, respectively. Each scenario was run with bioturbation, and the 2,300 and 7,000 Pg C scenarios were also run without bioturbation. Bioturbation is an important consideration because it would have re-supplied the surface sediments with $CaCO_3$ even as the CO_2 from the PETM pulse was dissolving $CaCO_3$ in those sediments. Thus, sediments that were bioturbated would have maintained higher wt% $CaCO_3$ than non-bioturbated sediments. Of the pulse sizes modeled in this study, 7,000 Pg C is the smallest that can reasonably reproduce the observed distribution of $CaCO_3$ during the PETM, but only if we allow that shallow sediments in the central equatorial Pacific were bioturbated during the PETM, and that deeper sediments in the Pacific and all sediments at Walvis Ridge in the southern Atlantic Ocean were not.

The second manuscript addresses a more basic issue: how well does the sedimentary record represent the actual $\delta^{13}C$ history of dissolved inorganic carbon (DIC) in seawater? This manuscript was motivated in part by the discrepancy between terrestrial and marine records of the PETM CIE. Which best reflects the excursion that actually occurred in the atmosphere: the -5 to -7‰ excursion on land, or the -4‰ excursion in the sea? Perhaps the marine sediments recorded smaller excursions because of the dissolution that occurred at the PETM. In this case, variable dissolution might explain the range of marine $\delta^{13}C$ excursions: at some sites the CIE is -4‰ or larger, whereas at others it is little more than -1‰. This would lead us to expect that the largest CIE magnitudes would occur at sites with the least dissolution. However, the data compiled for this study do not show a simple relationship between excursion magnitude and the change in wt% $CaCO_3$. In general, more of the larger excursions occur in sediments with a relatively small decrease in wt% $CaCO_3$, but some sites with near complete dissolution of $CaCO_3$ still record excursions of similar magnitude to sites with hardly any dissolution. Insights from modeling are used along with model sediment cores and $\delta^{13}C$ and $CaCO_3$ wt% observations to further elaborate on the nature of the PETM event.

The first of the two manuscripts was co-authored with Andy Ridgwell and Lee Kump and is being revised for further consideration by *Geology*. The second manuscript will be submitted to *Paleoceanography* and is co-authored with Andy Ridgwell, Lee Kump, and Tim Bralower. Andy provided assistance with modelling, and toward the end of the project took over running the final simulations with a new model version. Andy, Lee, and Tim have provided editorial assistance, and Tim has provided valuable guidance

in sorting through the literature on the PETM record in marine sediments. My contribution included taking the lead in writing both manuscripts, running the majority of the simulations, performing all post-processing tasks, and compiling PETM observations from the literature.

References

Bowen, G.J., Beerling, D.J., Koch, P.L., Zachos, J.C., and Quattlebaum, T., 2004, A humid climate state during the Palaeocene/Eocene thermal maximum: Nature, v. 432, p. 495-499.

Cramer, B.S., Aubry, M.-P., Miller, K.G., Olsson, R.K., Wright, J.D., and Kent, D.V., 1999, An exceptional chronologic, isotopic, and clay mineralogic record of the latest Paleocene thermal maximum, Bass River, NJ, ODP 174AX: Bulletin de la Societe Geologique de France, v. 170, p. 883-897.

Dickens, G.R., O'Neil, D., Rea, D.K., and Owen, R.M., 1995, Dissociation of oceanic methane hydrate as a cause of the carbon isotope excursion at the end of the Paleocene: Paleoceanography, v. 10, p. 965-971.

Edwards, N.R., and Marsh, R., 2005, Uncertainties due to transport-parameter sensitivity in an efficient 3-D ocean-climate model: Climate Dynamics, v. 24, p. 415-433.

Higgins, J.A., and Schrag, D.P., 2006, Beyond methane: Towards a theory for the Paleocene–Eocene Thermal Maximum: Earth and Planetary Science Letters, v. 245, p. 523-537.

Hunt, J.M., 1996, Petroleum geochemistry and geology: United States, W. H. Freeman and Company, New York, 743 p.

Kennett, J.P., and Stott, L.D., 1991, Abrupt deep-sea warming, palaeoceanographic changes and benthic extinctions at the end of the Paleocene: Nature, v. 353, p. 225-229.

Kent, D.V., Cramer, B.S., Lanci, L., Wang, D., Wright, J.D., and Van der Voo, R., 2003, A case for a comet impact trigger for the Paleocene/Eocene thermal maximum and carbon isotope excursion: Earth and Planetary Science Letters, v. 211, p. 13-26.

Kurtz, A.C., Kump, L.R., Arthur, M.A., Zachos, J.C., and Paytan, A., 2003, Early Cenozoic decoupling of the global carbon and sulfur cycles: Paleoceanography, v. 18, p. 14-1 - 14-14.

Lenton, T.M., Williamson, M.S., Edwards, N.R., Marsh, R., Price, A.R., Ridgwell, A.J., Shepherd, J.G., Cox, S.J., and team, T.G., 2006, Milennial timescale carbon cycle and climate change in an efficient Earth system model: Climate Dynamics, v. 26, p. 687-711.

Murphy, B., Lyle, M., and Olivarez Lyle, A., 2006, Biogenic burial across the Paleocene/ Eocene boundary: Ocean Drilling Program Leg 199 Site 1221, *in* Wilson, P.A., Lyle, M., and Firth, J.V., eds., Proc. ODP., Sci.Results, 199: College Station, TX (Ocean Drilling Program), 1-12. doi:10.2973/odp.proc.sr.199.215.2006

Pagani, M., Caldiera, K., Archer, D., and Zachos, J.C., 2006, An ancient carbon mystery: Science, v. 314, p. 1556-1557.

Ridgwell, A.J., 2001, Glacial-interglacial perturbations in the global carbon cycle [Ph.D. thesis], Univ. of East Anglia at Norwich, UK.

Ridgwell, A.J., and Hargreaves, J.C., 2007, Regulation of atmospheric CO_2 by deep-sea sediments in an Earth system model: Global Biogeochemical Cycles, v. 21, p. 14.

Ridgwell, A.J., Hargreaves, J.C., Edwards, N.R., Annan, J.D., Lenton, T.M., Yool, A., Marsh, R., and Watson, A.J., 2007, Marine geochemical data assimilation in an efficient Earth System Model of global biogeochemical cycling: Biogeosciences, v. 4, p. 87-104.

Rohl, U., Bralower, T.J., Norris, R.N., and Wefer, G., 2000, New chronology for the late Paleocene thermal maximum and its environmental implications: Geology, v. 28, p. 927-930.

Storey, M., Duncan, R.A., and Swisher, C.C.I., 2007, Paleocene-Eocene Thermal Maximum and the opening of the Northeast Atlantic: Science, v. 316, p. 587-589.

Svensen, H., Planke, S., Malthe-Sorenssen, Jamtveit, B., Myklebust, R., Rasmussen Eidem, T., and Rey, S.S., 2004, Release of methane from a volcanic basin as a mechanism for initial Eocene global warming: Nature, v. 429, p. 542-545.

Zachos, J.C., Rohl, U., Schellenberg, S., Sluijs, A., Hodell, D.A., Kelly, D.C., Thomas, E., Nicolo, M., Raffi, I., Lourens, L.J., McCarren, H., and Kroon, D., 2005, Rapid acidification of the ocean during the Paleocene-Eocene Thermal Maximum: Science, v. 308, p. 1611-1615.

Zachos, J.C., Wara, M.W., Bohaty, S., Delaney, M.L., Petrizzo, M.R., Brill, A., Bralower, T.J., and Premoli Silva, I., 2003, A transient rise in tropical sea surface temperature during the Paleocene-Eocene Thermal Maximum: Science, v. 302, p. 1551-1554.

Chapter 2

The sedimentary response to Paleocene Eocene Thermal Maximum carbon release: A model-data comparison[1]

Abstract

An Earth system model of intermediate complexity configured with early Eocene paleogeography is used to constrain possible sources of carbon that may have caused global warming at the Paleocene-Eocene boundary. We find that 7,000 Pg C with $\delta^{13}C$ of -22‰ is the smallest pulse modeled here to reasonably reproduce observations of seafloor $CaCO_3$ dissolution. This pulse is unlikely to have been the result of methane hydrate dissolution or mantle CO_2 from volcanic degassing alone, suggesting that additional sources of CO_2 such as from the oxidation of sedimentary organic carbon or thermogenic methane must also have contributed. Observed contrasts in dissolution intensity between Atlantic and Pacific sites are reproduced in the model by reducing bioturbation in the Atlantic, presumably associated with the spread of low-oxygen bottom waters.

---

[1] K. Panchuk, A. Ridgwell, and L. Kump, for submission to Geology.

Introduction

The Paleocene-Eocene boundary (55 Ma) was characterized by geologically abrupt global warming, with ocean temperatures rising by ~5 °C over as little as 10 ka (e.g., Kennett and Stott, 1991; Zachos et al., 2003; Sluijs et al., 2006). Marine sediments deposited during the Paleocene-Eocene Thermal Maximum (PETM) recorded an average carbon isotope ($\delta^{13}C$) excursion of -3‰ (e.g., Kennett and Stott, 1991; Zachos et al., 2003), as well as a marked decrease in calcium carbonate weight percent ($CaCO_3$ wt%; e.g., Thomas, 1998; Thomas et al., 1999; Zachos et al., 2005). The actual excursion was likely closer to -4‰ (e.g., Pagani et al., 2006), as recorded in well-preserved planktonic and benthic forams (Lu and Keller, 1993; Cramer et al., 1999; Thomas et al., 2002), although -5 to -7‰ excursions in terrestrial records suggest that it might have been even higher (e.g., Bowen et al., 2004 and references therein). In contrast, smaller (-2.5‰) excursions have been measured in bulk carbonates at Walvis Ridge (Zachos et al., 2005), where sediments undergo near complete dissolution. Together, the negative $\delta^{13}C$ excursion and $CaCO_3$ dissolution are consistent with the PETM being caused by a large pulse of ^{13}C-depleted carbon to the ocean or atmosphere (Dickens et al., 1995; Thomas and Shackleton, 1996). For this reason, the PETM has been viewed as an important possible analogue for the future consequences of fossil fuel burning.

The quantity of C needed from a potential source is constrained by its characteristic isotopic signature and the magnitude of the isotopic excursion, but these constraints cannot by themselves identify the actual source. Fortunately, more information is provided by the observed climatic and sedimentary response during the

PETM. Our approach to identifying the carbon source responsible for the PETM is to compare observed spatial and temporal variations in the $CaCO_3$ content of marine PETM sediments with predicted changes in the spatial distribution of $CaCO_3$ for three potential PETM scenarios: 1) biogenic methane (i.e., the methane clathrate hypothesis of Dickens et al., 1995), with $\delta^{13}C$ of -60‰; 2) rapid oxidation of sedimentary organic carbon (including peat as in Kurtz et al., 2003), with $\delta^{13}C$ of -22‰; and 3) massive addition of mantle-derived volcanic CO_2 with $\delta^{13}C$ of -5‰. These three scenarios do not represent all possible sources or combinations of sources, but they do span the range of source $\delta^{13}C$ values that have been suggested in the literature (e.g., Kent et al., 2003; Svensen et al., 2004; Storey et al., 2007).

This approach has only recently become possible with the development of intermediate complexity Earth system models. We use the GENIE-1 model (Lenton et al., 2006; Ridgwell et al., 2007; www.genie.ac.uk) to simulate climate, atmospheric composition, and marine biogeochemistry within a paleogeographically appropriate configuration while accounting for basic climate feedbacks. GENIE-1 is particularly valuable because the predicted spatial distribution of $CaCO_3$ burial and sea floor $CaCO_3$ $\delta^{13}C$ can be compared directly to geologic data describing the state of the Earth system before and during the PETM.

Methods

GENIE-1 includes the fast climate model of Edwards and Marsh (2005), consisting of a reduced physics (frictional geostrophic) 3-D ocean circulation model

(Edwards, 1996), coupled to a 2-D energy-moisture balance model (EMBM) of the atmosphere and a dynamic-thermodynamic sea-ice model based on that of Weaver et al. (2001). The ocean model includes a representation of marine carbon cycling (BIOGEM; Ridgwell et al., 2007), and, particularly important for interpreting the marine geological record, there is also a model of sea floor biogenic carbonate preservation (SEDGEM; Ridgwell and Hargreaves, 2007). In the model the $CaCO_3$ export from the ocean surface layer depends upon the $CaCO_3$:POC rain ratio parameter, the amount of $CaCO_3$ relative to particulate organic carbon (POC) exported as biogenic detritus from the surface ocean. POC export is itself a function of the PO_4^{3-} concentration in the ocean surface layer using a Monod growth formulation. POC and $CaCO_3$ are remineralized in the water column according to exponential decay functions. All POC reaching the sea floor is remineralized and returned to the ocean, however $CaCO_3$ which reaches the ocean floor is passed to the surface sediment layer of the sediment model. SEDGEM uses a look-up table generated by the model of Archer (1991) to determine how much sedimentary $CaCO_3$ dissolves. CO_2 evolved from the remineralization of POC is available to dissolve $CaCO_3$ within the sediments.

Sediment layers within SEDGEM are 1 cm thick. If the top layer is filled, SEDGEM moves the sediments down one layer. If all $CaCO_3$ in the top layer is dissolved, it is replaced by moving sediment layers up the column. In this way SEDGEM synthesizes a stratigraphic record that can be affected by the long-term depositional history of sea floor sediments. GENIE-1 was spun up for 150 ka to allow the system to reach geochemical equilibrium between weathering and sedimentation and to build up a sufficiently deep sedimentary column.

SEDGEM also allows for sediments to be bioturbated. Bioturbation is represented by mixing adjacent layers within the sediment stack. The rate of mixing is highest at the top of the stack, at 16 cm^2 /ka, and decreases down the stack of sediment layers according to an e-folding depth of 1 cm (Peng et al., 1979; Ridgwell, 2001). Bioturbation is important to consider because it acts as a source of $CaCO_3$ in the sediment surface layer, increasing the buffering capacity of the sediments for a given size of carbon pulse. Without bioturbation, the amount of $CaCO_3$ available for dissolution is limited by the initial $CaCO_3$ content of the sediments and the effective depth of diffusion. As $CaCO_3$ dissolves, detrital (non-carbonate) material accumulates and eventually forms a cap which prevents further dissolution of $CaCO_3$ deeper within the sediment column. The detrital flux to the sediments is 0.18 g cm^{-2} /ka, a value tuned to better approximate Latest Paleocene $CaCO_3$ wt% distributions. The non-carbonate detrital flux used here is still very similar to the value typical of the modern Pacific Ocean that was used in previous long-term fossil-fuel CO_2 removal simulations by Archer et al. (1998), 0.16 g cm^{-2} /ka.

The model has the early Eocene bathymetry and continental configuration of Bice et al. (1998; Appendix B) and the zonally averaged wind stress field of Bice and Marotzke (2002), both transformed to a 36×36 equal area model domain. A Late Paleocene pCO_2 level of 750 ppm was chosen because it gives model global average deep ocean temperatures close to temperatures derived from $\delta^{18}O$ analyses of benthic foraminifera, typically 11-12°C (Kennett and Stott, 1991; Bralower et al., 1995; Thomas et al., 2002), after the climate and ocean carbon cycle are equilibrated for 10,000 model years. An atmospheric CO_2 concentration of 750 ppm is within the range of proxy

studies and numerical models which have yielded estimates of Late Paleocene pCO_2 levels ranging from 300 ppm to >2000 ppm (Shellito et al., 2003 and references therein; Pagani et al., 2006).

The global weathering rate of HCO_3^- to the ocean and the $CaCO_3$:POC rain ratio are important sources of uncertainty because these parameters control the model $CaCO_3$ wt% distribution. We constrain these uncertainties by comparing the $CaCO_3$ wt% distribution from an ensemble of simulations reflecting a range of weathering rates and spatiotemporally uniform rain ratios to the observed Late Paleocene $CaCO_3$ wt%. All observations and their sources are summarized in Appendix B. It should be noted, however, that available data are biased toward carbonate-rich sediments because those sediments are often specifically targeted for drilling.

Another consideration when comparing data to model results is that $CaCO_3$ wt% is topographically controlled, so the coarse bathymetric grid means that data sites do not always correspond to model cells of the appropriate depth. There is also substantial uncertainty associated with sediment paleodepths and with the reconstructed location of Late Paleocene spreading ridges. Thus, we would not *a priori* expect to achieve a perfect model-data fit at all sites. We address this problem for both initial conditions and PETM simulations by plotting $CaCO_3$ wt% versus depth for a subset of grid cells surrounding data-rich sites. The best match is determined by finding the ensemble member with the minimum root mean square error (RMSE). This process is detailed in Appendix C.

We assess the geochemical impacts of three possible carbon sources: the "methane" scenario, in which biogenic methane from clathrates (-60‰) is presumed to oxidize immediately to CO_2; the "organic C" scenario (-22‰); and the "volcanic CO_2"

scenario (-5‰). The amount of CO_2 added in each case is that which instantaneously decreases the $\delta^{13}C$ of the combined atmosphere and ocean carbon reservoir by 4‰. Following Dickens (2003), CO_2 was applied uniformly to the atmosphere over 10 ka, then the model was run for an additional 100 ka without CO_2 flux forcing. For the methane, organic C, and volcanic CO_2 scenarios, 2,300, 7,000, and 70,000 Pg C, respectively, were added. The methane and organic C scenarios were run twice: once without bioturbation of the sediments, and once with bioturbation. Three intermediate scenarios with bioturbation on were also run to populate the gap between 7,000 Pg C and 70,000 Pg C. Pulses of 15,000, 21,000, and 46,000 Pg C were added, reflecting carbon sources with $\delta^{13}C$ of -12‰, -9.5‰, and -6‰, respectively.

Results and Discussion

Initial Late Paleocene conditions

Observations suggest that the pre-PETM calcite compensation depth (CCD), the depth at which $CaCO_3$ is no longer found in sediments, was ~3500 to 4000 m or below in the data-rich regions of the central equatorial Pacific, Walvis Ridge in the Atlantic Ocean, and the southern Indian Ocean (regions a, b, and c, respectively in Fig. 2-1). The weathering flux – rain ratio ensemble member best fitting the observations has a $CaCO_3$:POC rain ratio of 0.175, somewhat higher than estimates of the modern global average (e.g., 0.06, Sarmiento et al., 2002; 0.14, Ridgwell et al., 2007), and a total global weathering rate of 50 Tmol HCO_3^- a^{-1}, which is larger than the 23-39 Tmol HCO_3^- a^{-1}

modern estimate (Munhoven, 2002) but less than Early Eocene model simulations (>70 Tmol HCO_3^- a^{-1}, Gibbs et al, 1999). Some specific sites, particularly in the Indian Ocean, are difficult to reproduce. This may reflect regional deficiencies in ocean circulation and/or biogeochemistry, or the fact that the coarse bathymetry does not permit sufficiently detailed representations of rapidly sloping regions.

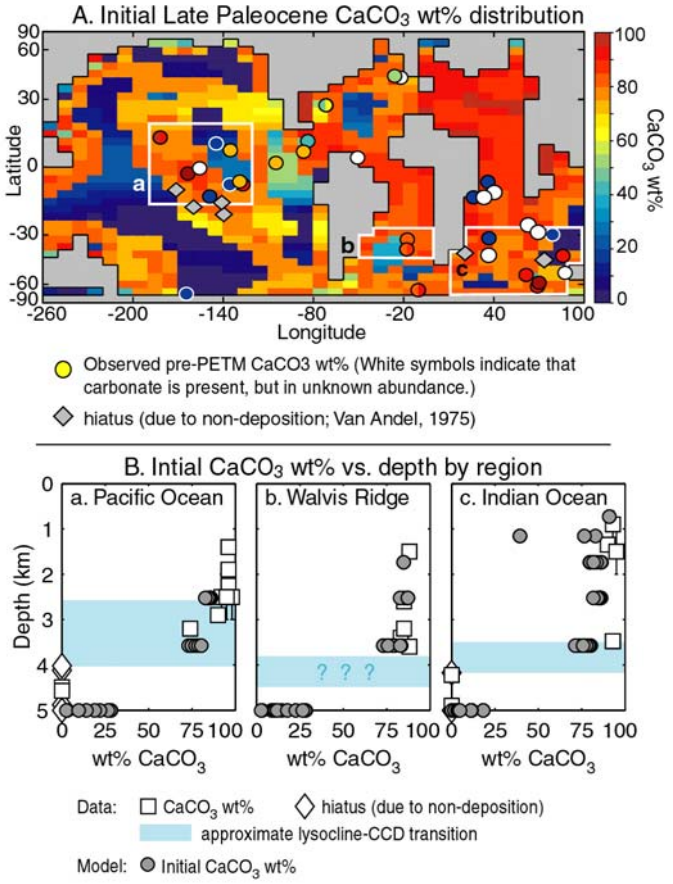

Figure 2-1: Pre-PETM model $CaCO_3$ wt% plotted in map view (A) and versus depth (B), both with observations superimposed. Results in B are plotted for data-rich regions delineated in A by white boxes. These are: a) the central equatorial Pacific Ocean, b) Walvis Ridge, and c) the southern Indian Ocean. See Appendix A for data values and sources.

The circulation state of the deep ocean has been traced through gradients of benthic foraminiferal $\delta^{13}C$ (e.g., Nunes and Norris, 2005; Tripati and Elderfield, 2005). With atmospheric CO_2 $\delta^{13}C$ set at -6‰ we obtain model bottom water $\delta^{13}C$ values which are consistent with those compiled by Nunes and Norris (2006; Fig. 2-2). Data and our model results show a decreasing $\delta^{13}C$ gradient from the southern Atlantic toward the northern Atlantic, and from the Indian Ocean toward the Pacific, from which a dominant Southern Ocean deep-water source region has been inferred for the Late Paleocene. Nd isotopic records also support this interpretation, and suggest an intermediate water source in the North Pacific (Thomas et al., 2003) which is predicted by the model as well. Thus, despite the low spatial resolution of the ocean model and lack of a dynamic atmosphere, initial model circulation patterns are not inconsistent with data-based interpretations of Late Paleocene circulation patterns.

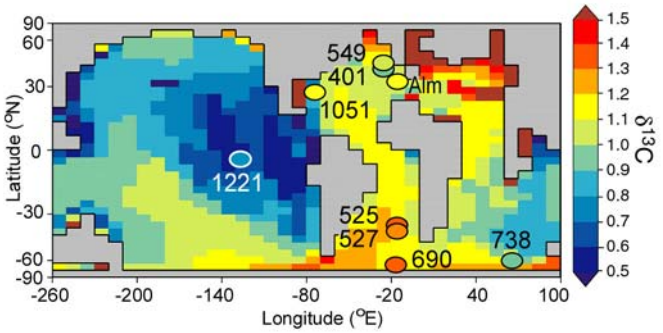

Figure 2-2: Model bottom water DIC $\delta^{13}C$ with observations as compiled by Nunes and Norris (2006) superimposed (circular markers).

PETM results

Globally averaged whole ocean temperatures increased by ~1.5, 4, and 14°C for the methane, organic C, and volcanic CO_2 cases, respectively (Fig. 2-3B), corresponding to increases in atmospheric CO_2 from 750 to 1,140, 2,200, and 25,500 ppm, respectively (Fig 2-3C). The larger the CO_2 pulse, the more sea floor $CaCO_3$ wt% decreases (Fig.2-3D). In the case of the 70,000 Pg C volcanic CO_2 pulse, $CaCO_3$ is completely dissolved over the entire sea floor, severely over-predicting $CaCO_3$ dissolution. The effect of bioturbation is apparent for the 2,300 and 7,000 Pg C pulses. When sediments are bioturbated (dashed lines in Fig. 2-3D) globally averaged $CaCO_3$ wt% is higher at the PETM than for non-bioturbated sediments (solid lines in Fig. 2-3D), and the peak PETM atmospheric CO_2 level is slightly lower for bioturbated sediments than non-bioturbated sediments (black lines in Fig. 2-3C), reflecting the enhanced buffering capacity afforded by a continuous re-supply of $CaCO_3$ to the surface sediment layer by bioturbation.

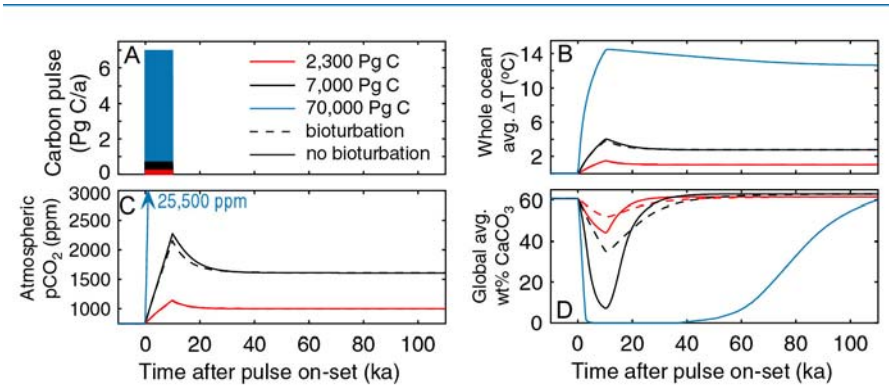

Figure 2-3: Timeseries plots of model output.

Our model does not predict substantial reversal in circulation or weakening of Southern source water production in response to PETM warming, contrary to the interpretation of Nunes and Norris (2006), but in agreement with Bice and Marotzke (2002).

Maps of $CaCO_3$ wt% results from immediately after the 10 ka pulse (Fig. 2-4) and regional plots of $CaCO_3$ wt% versus depth (Fig. 2-5) show that no one scenario can

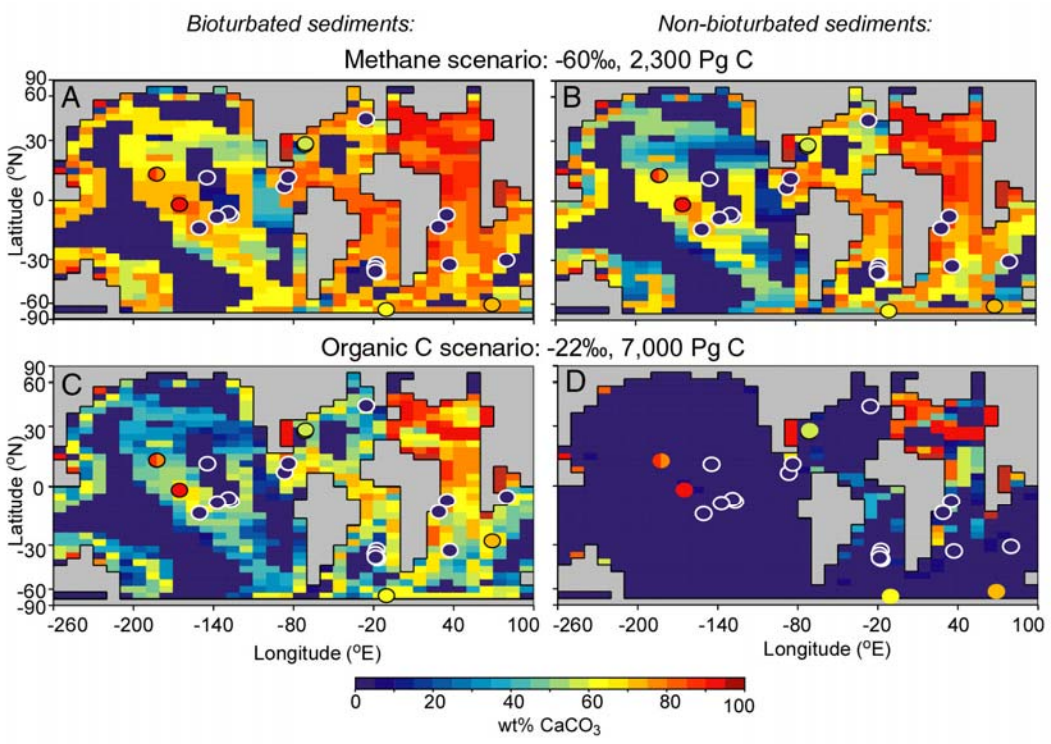

Figure 2-4: Model PETM $CaCO_3$ wt% with observations superimposed (circular markers). The 70,000 Pg C case is not shown in this figure because there is no $CaCO_3$ left in the sediments. See Appendix A for data values and sources.

reproduce all of the features of the PETM $CaCO_3$ wt% distribution. In the central equatorial Pacific region, data suggest a CCD at < 3,000 m depth, but sediments from the slightly shallower sites at ~ 2,500 m depth (from Shatsky Rise) retain > 75 wt% $CaCO_3$.

At Walvis Ridge the CCD appears < 1,500 m deep, resulting in 0 wt% $CaCO_3$ at all Walvis Ridge sites during the PETM. The model, however, displays approximately the same response in both basins. Therefore, the > 75 wt% $CaCO_3$ in the Pacific can be reproduced by the methane scenarios (Fig. 2-5A), but only at the cost of substantially over-estimating the $CaCO_3$ content deeper in the Pacific and at Walvis Ridge (Fig. 2-5A,B; we note, however, that our initial scenario underestimates the $CaCO_3$ wt% at the shallow Pacific sites by 10%). Alternatively, a 7,000 Pg C pulse in the absence of

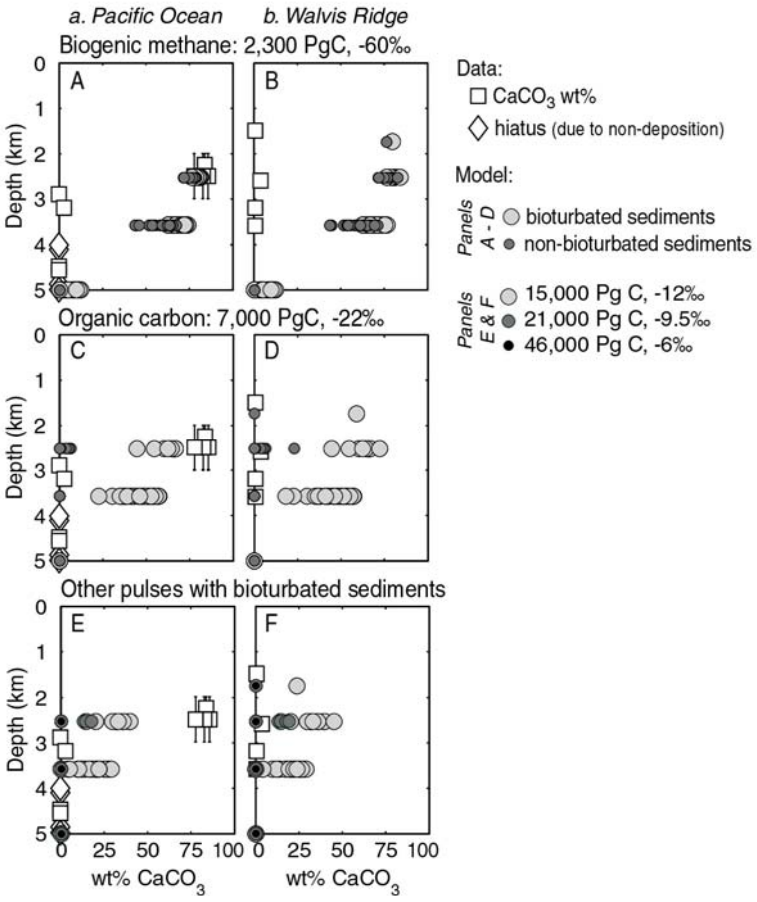

Figure 2-5: PETM model $CaCO_3$ wt% plotted versus depth with observations superimposed. Results are plotted for data-rich regions of the central equatorial Pacific Ocean (left column) and Walvis Ridge (right column; regions a and b, respectively in Fig. 2-1A).

bioturbation will reproduce the 0 wt% $CaCO_3$ at depths >3,000 m in the Pacific, and at Walvis Ridge, but only at the cost of losing all $CaCO_3$ at the 2,500 m sites in the Pacific (Fig. 2-5C,D).

This trade-off is apparent in the distribution of RMSE (Fig. 2-6). For the Pacific region the RMSE is lowest for the 15,000 Pg C pulse with bioturbation (Fig. 2-6A), striking a compromise with 0 wt% $CaCO_3$ at the 3,600 m model layer, and 20 - 50 wt% $CaCO_3$ at the 2,500 m model layer. For Walvis Ridge any scenario that dissolves all $CaCO_3$ will have RMSE of 0. Three scenarios satisfy this requirement: 7,000 Pg C without bioturbation, and 46,000 and 70,000 Pg C with bioturbation (Fig. 2-6B). The sum of the Pacific and Walvis Ridge distributions yields two minima: one for 7,000 Pg C without bioturbation, and the other for 21,000 Pg C with bioturbation (Fig. 2-6C).

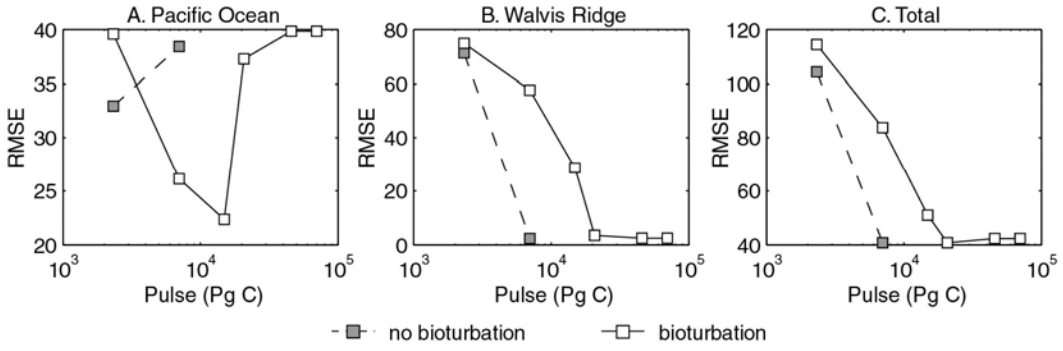

Figure 2-6: Evaluation of model outcomes by comparison of root mean squared errors (RMSE).

One way to reconcile these results is to allow for a decrease in the strength of bioturbation during the PETM at Walvis Ridge and at the deeper Pacific sites. In general, evidence appears to suggest that this was the case at Sites 1220 and 1221 in the Pacific (Shipboard Scientific Party, 2002; Murphy et al., 2006) at paleodepths of 2,900 and

3,200 m, respectively (Rea and Lyle, 2005), and at Walvis Ridge (Shipboard Scientific Party, 2002, 2004b, a). In contrast, sediments at the shallower Pacific Shatsky Rise sites have been reported as "strongly bioturbated" (Colosimo et al., 2006).

What caused the PETM?

Allowing that spatiotemporal variations in the rate of bioturbation can account for the very different responses of the central equatorial Pacific and Walvis Ridge sediments during the PETM, 7,000 Pg C is the smallest pulse modeled here that dissolves enough $CaCO_3$ to reasonably reproduce observations. The 2,300 Pg C pulse of biogenic methane causes only a small decrease in $CaCO_3$ wt%, whether bioturbation is present or not. This result is in agreement with Zachos et al. (2005), who concluded that a pulse derived solely from biogenic methane would dissolve insufficient $CaCO_3$. Our result also offers an alternative to the very high climate sensitivity to CO_2 doubling, 6.8 to 7.8°C, estimated to be necessary to generate PETM warming and a -3 to -5‰ $\delta^{13}C$ excursion with biogenic methane (Pagani et al., 2006). If 7,000 Pg C is the lower bound on pulse size (given that 7,000 Pg C without bioturbation is the smallest pulse to simulate complete dissolution in the Atlantic, but 15,000 Pg C is the best fit to the Pacific data), then the upper bound on climate sensivity is reduced to 4°C (Fig. 2 of Pagani et al., 2006). Pulses of 21,000 Pg C and greater decrease $CaCO_3$ wt% too much in our model; the climate sensitivity to CO_2 doubling corresponding to an upper bound on pulse size of 21,000 Pg C is 2.5°C.

A pulse of 7,000 Pg C with $\delta^{13}C$ of -22‰ is generally consistent with the hypotheses that organic carbon was released to the atmosphere by peat fires (Kurtz et al., 2003), or by weathering of fossil carbon (Higgins and Schrag, 2006). Alternatively, it could reflect a combination of volcanic CO_2 (i.e., mantle-derived CO_2 with $\delta^{13}C$ of -5‰) and thermogenic methane ($\delta^{13}C$ of -35 to -50‰, Hunt, 1996) evolved during the emplacement of the North Atlantic Igneous Province. (NAIP; Svensen et al., 2004; Storey et al., 2007). The timing of the PETM appears to coincide with massive eruptions of flood basalts and the emplacement of sill complexes associated with the rifting between Greenland and Europe (Svensen et al., 2004; Storey et al., 2007). NAIP formation is estimated to have yielded between 1,500 and 15,000 Pg C of thermogenic methane (Svensen et al., 2004), so it is not entirely unreasonable that 2,600 to 4,000 Pg C might have been derived from thermogenic methane (with $\delta^{13}C$ of -35 and -50‰, respectively), and mixed with higher $\delta^{13}C$ CO_2 from basalt degassing.

NAIP volcanism may turn out to be a very economical explanation for the events of the Late Paleocene and the Eocene, accounting for long-term warming, possibly accounting for the PETM, and given that melt production lasted well into the Eocene (Storey et al., 2007), intervals of relatively high rates of melt production may account for PETM-like Eocene hyperthermal events (e.g., Lourens et al., 2005). The NAIP volcanism hypothesis offers the distinct advantage of being relatively easy to test by dating and correlation of volcanic ash layers (e.g., Storey et al., 2007).

Conclusion

In our simulations of the Paleocene-Eocene Earth system, a pulse of 7,000 Pg C with $\delta^{13}C$ of -22‰ comes closest to reproducing the changes in sea floor $CaCO_3$ distribution that took place during the PETM, but it is necessary to permit differences in the rate of bioturbation of Pacific and Atlantic Ocean sediments. A $\delta^{13}C$ of -22‰ is consistent with sedimentary organic carbon, or a combination of volcanic degassing and thermogenic methane.

Acknowledgements

This paper represents part of Panchuk's Ph.D. work at Penn State. We wish to thank Robert Marsh and Andrew Yool for setting up the Eocene configuration of the GENIE-1 climate model, and Karen Bice, Jerry Dickens, and an anonymous reviewer for helpful comments on an earlier version of the manuscript. We are very grateful to Tim Bralower, Klaus Keller, and Ray Najjar for their careful reading of the manuscript, detailed written comments, and thoughtful discussions. This work was funded by a Worldwide Universities Network travel grant to Panchuk, Canadian Foundation for Climate and Atmospheric Sciences funding to Ridgwell, and an NSF Biocomplexity grant to Kump.

References

Archer, D., 1991, Modeling the calcite lysocline: Journal of Geophysical Research, v. 96, p. 17037-17050.

Archer, D., Kheshgi, H.S., and Maier-Reimer, E., 1998, Dynamics of fossil fuel CO_2 neutralization by marine $CaCO_3$: Global Biogeochemical Cycles, v. 12, p. 259-276.

Bice, K.L., Barron, E.J., and Peterson, W.H., 1998, Reconstruction of realistic early Eocene paleobathymetry and ocean GCM sensitivity to specified basin configuration, *in* Crowley, T., and Burke, K., eds., Tectonic Boundary Conditions for Climate Reconstructions: New York, Oxford University Press, p. 227-247.

Bice, K.L., and Marotzke, J., 2002, Could changing ocean circulation have destabilized methane hydrate at the Paleocene/Eocene boundary?: Paleoceanography, v. 17.

Bowen, G.J., Beerling, D.J., Koch, P.L., Zachos, J.C., and Quattlebaum, T., 2004, A humid climate state during the Palaeocene/Eocene thermal maximum: Nature, v. 432, p. 495-499.

Bralower, T.J., Parrow, M., Thomas, E., and Zachos, J.C., 1995, Data Report: Stable isotopic stratigraphy of the Paleogene pelagic cap at Site 865, Allison Guyot, *in* Winterer, E.L., Sager, W.W., Firth, J.V., and Sinton, J.M., eds., Proceedings of the Ocean Drilling Program, Scientific Results, Volume 143: College Station, TX (Ocean Drilling Program), p. 581-586.

Colosimo, A., Bralower, T.J., and Zachos, J.C., 2006, Evidence for lysocline shoaling at the Paleocene/Eocene Thermal Maximum on Shatsky Rise, Northwest Pacific, *in* Bralower, T.J., Premoli Silva, I., and Malone, M., eds., Proc. ODP., Sci. Results, 198: College Station, TX (Ocean Drilling Program), 1-36. doi:10.2973/odp.proc.sr.198.112.2006

Cramer, B.S., Aubry, M.-P., Miller, K.G., Olsson, R.K., Wright, J.D., and Kent, D.V., 1999, An exceptional chronologic, isotopic, and clay mineralogic record of the latest Paleocene thermal maximum, Bass River, NJ, ODP 174AX: Bulletin de la Societe Geologique de France, v. 170, p. 883-897.

Dickens, G.R., 2003, Rethinking the global carbon cycle with a large, dynamic and microbially mediated gas hydrate capacitor: Earth and Planetary Science Letters, p. 14.

Dickens, G.R., O'Neil, D., Rea, D.K., and Owen, R.M., 1995, Dissociation of oceanic methane hydrate as a cause of the carbon isotope excursion at the end of the Paleocene: Paleoceanography, v. 10, p. 965-971.

Edwards, N.R., 1996, Unsteady similarity solutions and oscillating ocean gyres: Journal of Marine Research, v. 54, p. 793-826.

Edwards, N.R., and Marsh, R., 2005, Uncertainties due to transport-parameter sensitivity in an efficient 3-D ocean-climate model: Climate Dynamics, v. 24, p. 415-433.

Gibbs, M.T., Bluth, G.J.S., Fawcett, P.J., and Kump, L.R., 1999, Global chemical erosion over the last 250 My: variations due to changes in paleogeography, paleoclimate, and paleogeology: American Journal of Science, v. 299, p. 611-651.

Higgins, J.A., and Schrag, D.P., 2006, Beyond methane: Towards a theory for the Paleocene–Eocene Thermal Maximum: Earth and Planetary Science Letters, v. 245, p. 523-537.

Kennett, J.P., and Stott, L.D., 1991, Abrupt deep-sea warming, palaeoceanographic changes and benthic extinctions at the end of the Paleocene: Nature, v. 353, p. 225-229.

Kent, D.V., Cramer, B.S., Lanci, L., Wang, D., Wright, J.D., and Van der Voo, R., 2003, A case for a comet impact trigger for the Paleocene/Eocene thermal maximum and carbon isotope excursion: Earth and Planetary Science Letters, v. 211, p. 13-26.

Kurtz, A.C., Kump, L.R., Arthur, M.A., Zachos, J.C., and Paytan, A., 2003, Early Cenozoic decoupling of the global carbon and sulfur cycles: Paleoceanography, v. 18, p. 14-1 - 14-14.

Lenton, T.M., Williamson, M.S., Edwards, N.R., Marsh, R., Price, A.R., Ridgwell, A.J., Shepherd, J.G., Cox, S.J., and team, T.G., 2006, Milennial timescale carbon cycle and climate change in an efficient Earth system model: Climate Dynamics, v. 26, p. 687-711.

Lourens, L.J., Sluijs, A., Kroon, D., Zachos, J.C., Thomas, E., Rohl, U., Bowles, J., and Raffi, I., 2005, Astronomical pacing of late Palaeocene to early Eocene global warming events: Nature, v. 435, p. 1083-1087.

Lu, G., and Keller, G., 1993, The Paleocene-Eocene transition in the Antarctic Indian Ocean: Inference from planktonic foraminifera: Marine Micropaleontology, v. 21, p. 101-142.

Munhoven, G., 2002, Glacial–interglacial changes of continental weathering: estimates of the related CO_2 and HCO_3^- f lux variations and their uncertainties: Global and Planetary Change, v. 33, p. 155-176.

Murphy, B., Lyle, M., and Olivarez Lyle, A., 2006, Biogenic burial across the Paleocene/ Eocene boundary: Ocean Drilling Program Leg 199 Site 1221, *in* Wilson, P.A., Lyle, M., and Firth, J.V., eds., Proc. ODP., Sci.Results, 199: College Station, TX (Ocean Drilling Program), 1-12. doi:10.2973/odp.proc.sr.199.215.2006

Nunes, F., and Norris, R.N., 2005, Data report: High-resolution stable isotope records across the Paleocene/ Eocene boundary, ODP Sites 1220 and 1221, *in* Wilson, P.A., Lyle, M., and Firth, J.V., eds., Proc. ODP, Sci. Results, 199, 1–12 [CD-ROM].

—, 2006, Abrupt reversal in ocean overturning during the Palaeocene/ Eocene warm period: Nature, v. 439, p. 60-63.

Pagani, M., Caldiera, K., Archer, D., and Zachos, J.C., 2006, An ancient carbon mystery: Science, v. 314, p. 1556-1557.

Peng, T.-H., Broecker, W.S., and Berger, W.H., 1979, Rates of benthic mixing in deep-sea sediment as determined by radioactive tracers: Quaternary Research, v. 11, p. 141-149.

Rea, D.K., and Lyle, M., 2005, Paleogene calcite compensation depth in the eastern subtropical Pacific: Answers and questions: Paleoceanography, v. 20, p. 9.

Ridgwell, A.J., 2001, Glacial-interglacial perturbations in the global carbon cycle [Ph.D. thesis], Univ. of East Anglia at Norwich, UK.

Ridgwell, A.J., and Hargreaves, J.C., 2007, Regulation of atmospheric CO_2 by deep-sea sediments in an Earth system model: Global Biogeochemical Cycles, v. 21, p. 14.

Ridgwell, A.J., Hargreaves, J.C., Edwards, N.R., Annan, J.D., Lenton, T.M., Yool, A., Marsh, R., and Watson, A.J., 2007, Marine geochemical data assimilation in an efficient Earth System Model of global biogeochemical cycling: Biogeosciences, v. 4, p. 87-104.

Sarmiento, J.L., Dunne, J., Gnanadesikan, A., Key, R.M., Matsumoto, K., and Slater, R., 2002, A new estimate of the $CaCO_3$ to organic carbon export ratio: Global Biogeochemical Cycles, v. 16, p. 12.

Shellito, C.J., Sloan, L.C.S., and Huber, M., 2003, Climate model sensitivity to atmospheric CO2 levels in the Early -Middle Paleogene: Palaeogeography, Palaeoclimatology, Palaeoecology, v. 193, p. 113-123.

Shipboard Scientific Party, 2002, Site 1220, *in* Lyle, M., Wilson, P.A., Janecek, T., et al., eds., Proc. ODP, Init. Repts., 199: College Station, TX (Ocean Drilling Program), 1-93. doi:10.2973/odp.proc.ir.199.113.2002

—, 2004a, Site 1263, *in* Zachos, J.C., Kroon, D., Blum, J.D., et al., eds., Proc. ODP, Init. Repts., 208: College Station, TX (Ocean Drilling Program), 1-87. 10.2973/odp.proc.ir.208.104.2004

—, 2004b, Site 1266, *in* Zachos, J.C., Kroon, D., Blum, J.D., et al., eds., Proc. ODP, Init. Repts., 208: College Station, TX (Ocean Drilling Program), 1-79. 10.2973/odp.proc.ir.208.107.2004

Sluijs, A., Schouten, S., Pagani, M., Woltering, M., Brinkhuis, H., Sinninghe Damste, J.S., Dickens, G.R., Huber, M., Reichart, G.-J., Stein, R., Matthiessen, J., Lourens, L.J., Pedentchouk, N., Backman, J., Moran, K., and Scientists, E., 2006, Subtropical Arctic Ocean temperatures during the Palaeocene/ Eocene thermal maximum: Nature, v. 441, p. 610-613.

Storey, M., Duncan, R.A., and Swisher, C.C.I., 2007, Paleocene-Eocene Thermal Maximum and the opening of the Northeast Atlantic: Science, v. 316, p. 587-589.

Svensen, H., Planke, S., Malthe-Sorenssen, Jamtveit, B., Myklebust, R., Rasmussen Eidem, T., and Rey, S.S., 2004, Release of methane from a volcanic basin as a mechanism for initial Eocene global warming: Nature, v. 429, p. 542-545.

Thomas, D.J., Bralower, T.J., and Jones, C.E., 2003, Neodymium isotopic reconstruction of late Paleocene-early Eocene thermohaline circulation: Earth and Planetary Science Letters, v. 209, p. 309-322.

Thomas, D.J., Bralower, T.J., and Zachos, J.C., 1999, New evidence for subtropical warming during the late Paleocene thermal maximum: Stable isotopes from Deep Sea Drilling Project Site 527, Walvis Ridge: Paleoceanography, v. 14, p. 561-570.

Thomas, D.J., Zachos, J.C., Bralower, T.J., Thomas, E., and Bohaty, S., 2002, Warming the fuel for the fire: Evidence for thermal dissociation of methane hydrate during the Paleocene-Eocene thermal maximum: Geology, v. 30, p. 1067-1070.

Thomas, E., 1998, Biogeography of the Late Paleocene Benthic Foraminiferal Extinction, *in* Aubry, M.-P., Lucas, S.G., and Berggren, W.A., eds., Late Paleocene-Early Eocene Climatic and Biotic Events in the Marine and Terrestrial Records: New York, Columbia University Press, p. 214–243.

Thomas, E., and Shackleton, N.J., 1996, The Paleocene-Eocene benthic foraminiferal extinction and stable isotope anomalies, *in* Knox, R.W.O.B., Corfield, R.M., and Dunay, R.E., eds., Correlation of the Early Paleogene in Northwest Europe, Geological Society Special Publication No. 101, p. 401-441.

Tripati, A., and Elderfield, H., 2005, Deep-sea temperature and circulation changes at the Paleocene-Eocene thermal maximum: Science, v. 308, p. 1894-1898.

Weaver, A.J., Eby, M., Wiebe, E.C., Bitz, C.M., Duffy, P.B., Ewen, T.L., Fanning, A.F., Holland, M.M., MacFayden, A., Saenko, O., Schmittner, A., Wang, H., and Yoshimori, M., 2001, The UVic Earth System Climate Model: Model description, climatology, and applications to past, present, and future climates: Atmosphere-Ocean, v. 39, p. 68.

Zachos, J.C., Rohl, U., Schellenberg, S., Sluijs, A., Hodell, D.A., Kelly, D.C., Thomas, E., Nicolo, M., Raffi, I., Lourens, L.J., McCarren, H., and Kroon, D., 2005, Rapid acidification of the ocean during the Paleocene-Eocene Thermal Maximum: Science, v. 308, p. 1611-1615.

Zachos, J.C., Wara, M.W., Bohaty, S., Delaney, M.L., Petrizzo, M.R., Brill, A., Bralower, T.J., and Premoli Silva, I., 2003, A transient rise in tropical sea surface temperature during the Paleocene-Eocene Thermal Maximum: Science, v. 302, p. 1551-1554.

Chapter 3

Differences between the carbon isotope history of ocean surface water and the sedimentary record of carbon isotopic excursions during the Paleocene-Eocene Thermal Maximum: A model study[2]

Abstract

We find that bioturbation and the rate of recovery of the saturation state of seawater are key factors influencing the magitude of the recorded marine $\delta^{13}C$ excursion as well as the record of changes in $CaCO_3$ wt%. We conclude that, while the marine $\delta^{13}C$ excursion and $CaCO_3$ wt% records may not be consistently reliable indicators of the amount and $\delta^{13}C$ of the carbon added to the Earth system to cause the PETM, the timescales of the system recovery as indicated by those records might be. Differences in these timescales from one site to another may also provide valuable information about the response of the Earth system to PETM climate change.

Introduction

Mass balance calculations have been used to determine the carbon source that caused the Paleocene-Eocene Thermal Maximum (PETM) event: given the carbon isotopic composition ($\delta^{13}C$) of possible sources, how much carbon from a particular

---

[2] K. Panchuk, A. Ridgwell, L. Kump, and T. Bralower, for submission to Paleoceanography.

source would be required to produce the carbon isotopic excursion (CIE) observed in the Latest Paleocene ocean-atmosphere system, and is that quantity consistent with our understanding of the state of the Earth system at that time? A unique solution has not come of this approach because there are many combinations of $\delta^{13}C$ and pulse size that could provide the right excursion. Additional constraints may be brought to bear on the problem, such as spatial and temporal changes in the distribution of $CaCO_3$ sediments (Chapter 2). However, uncertainty regarding the magnitude of the PETM CIE itself remains to be addressed (e.g., Pagani et al., 2006).

There is a puzzling discrepancy in the magnitude of the PETM CIE recorded in terrestrial versus marine environments. On land the CIE is -5 to -7‰ (Bowen et al., 2004 and references therein), whereas foraminifera from marine sediments display average excursions of -3 to -4‰ (Table 3-1). The terrestrial $\delta^{13}C$ excursions may have been amplified relative to the marine by increased turnover of organic matter in soils and increased isotopic discrimination during photosynthesis under conditions of higher relative humidity (Bowen et al., 2004). However, this does not explain the range of excursions in the marine record, from -1‰ to larger than -4‰ (Table 3-1). $CaCO_3$ dissolution might account for this variability; dissolution and/or lack of deposition of sediments is characteristic of the PETM, although $CaCO_3$ wt% varies widely, with relatively little change in the $CaCO_3$ content of sediments at some locations (e.g., Shatsky Rise in the Pacific Ocean, Colosimo et al., 2006), but complete dissolution of $CaCO_3$ at others (e.g., Walvis Ridge in the Atlantic, Zachos et al., 2005).

Table 3-1: $\delta^{13}C$ values of planktonic foraminifera and bulk $CaCO_3$

Location	Material	$\delta^{13}C$		Source
		baseline	excursion	
Pacific Ocean				
Kerguelen Plateau (Site 738)	*A. soldadoensis*	3.8	-4.0	Lu and Keller (1993)
Shatsky Rise				
1209	*M. velascoensis*	4.0	-3.2	Zachos et al. (2003)
	A. soldadoensis	4.0	-3.7	Zachos et al. (2003)
	bulk $CaCO_3$	2.8	-2.5	Colosimo et al. (2006)
1210	bulk $CaCO_3$	2.6	-2.1	Colosimo et al. (2006)
1211	bulk $CaCO_3$	2.9	-2.7	Colosimo et al. (2006)
1212	bulk $CaCO_3$	3.2	-2.7	Colosimo et al. (2006)
Equatorial Pacific				
1220	bulk $CaCO_3$	1.0	-0.6	Nunes and Norris (2005)
1221	bulk $CaCO_3$	1.9	-0.9	Nunes and Norris (2005)
Caribbean Sea				
Nicaraguan Rise (Site 1001)	bulk $CaCO_3$	2.0	-3.0	Bralower et al. (1997)
Atlantic Ocean				
Bay of Biscay (Site 401)	*M. subbotinae*	4.3	-2.0	Pardo et al. (1997)
Goban Spur (Site 549)	*M. subbotinae*	4.7	-4.5	Stott et al. (1996)
Blake Nose (Site 1051)	bulk $CaCO_3$	2.2	-1.6	Bains et al. (1999)
Walvis Ridge				
525	bulk $CaCO_3$	2.4	-2.5	Thomas and Shackleton (1996)
1262	bulk $CaCO_3$	2.3	-2.2	Zachos et al. (2005)
1263	bulk $CaCO_3$	2.0	-2.9	Zachos et al. (2005)
1265	bulk $CaCO_3$	2.2	-2.7	Zachos et al. (2005)
1266	bulk $CaCO_3$	2.1	-2.0	Zachos et al. (2005)
1267	bulk $CaCO_3$	2.2	-2.6	Zachos et al. (2005)
Southern Ocean				
Maud Rise				
689	*A. mckannai*	2.9	-2.9	Thomas and Shackleton (1996)
690	*Acarinina*	3.2	-4.0	Thomas et al. (2002)
	bulk $CaCO_3$	2.9	-2.8	Bains et al. (1999)

If smaller $\delta^{13}C$ excursions reflect gaps in the sedimentary record, we would expect to see that smaller excursions occur at sites with greater decreases in $CaCO_3$, but this is not obvious in the published data (Fig. 3-1; locations are shown in Fig. 3-2). In Fig. 3-1A, the CIE magnitudes in planktonic foraminiferal records and bulk carbonate are plotted against the decrease in $CaCO_3$ wt% normalized to pre-PETM values, $\Delta_n CaCO_3$:

$$\Delta_n CaCO_3 = \frac{CaCO_{3,initial} - CaCO_{3,final}}{CaCO_{3,initial}} \qquad \text{(Eq. 3-1)}$$

where $CaCO_{3,initial}$ and $CaCO_{3,final}$ are the $CaCO_3$ wt% for a site before the PETM and at the peak of the PETM, respectively. For sediments with $CaCO_3$ prior to the PETM, but none during the PETM, $\Delta_n CaCO_3 = 1$. The advantage of this formulation is that it distinguishes between cases with the same change in $CaCO_3$ wt%, but different initial $CaCO_3$ wt%. In other words, sites where $CaCO_3$ wt% decreases from 80% to 60% and from 50% to 30% both have decreases of 20 wt% $CaCO_3$, but more $CaCO_3$ is dissolved in the former case than in the latter.

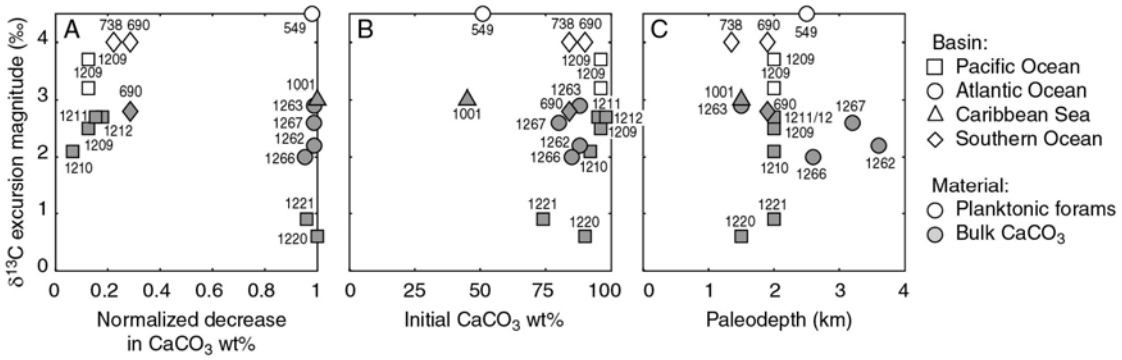

Figure 3-1: $\delta^{13}C$ excursion magnitude in planktonic foraminifera and bulk $CaCO_3$ versus: A) the decrease in $CaCO_3$ wt% normalized to initial values; B) initial $CaCO_3$ wt%; C) paleodepth. Data are labeled with DSDP/ ODP site numbers. See Appendix A for data and sources.

In general, more sites with larger excursions do show a smaller decrease in $CaCO_3$, but there is remarkably little difference between the bulk $CaCO_3$ CIE magnitudes at Walvis Ridge (Sites 1262 – 1267), where $\Delta_n CaCO_3 \sim 1$, and those at Shatsky Rise (Sites 1209 - 1212) and Maud Rise (Site 690) where $\Delta_n CaCO_3 < 0.3$. Another interesting feature of Fig. 3-1A is that, for $\Delta_n CaCO_3$ up to ~ 0.3, CIE magnitudes appear to increase rather than decrease as $\Delta_n CaCO_3$ increases. At Site 1209 the excursion magnitudes in planktonic foraminifera are 3.2 and 3.7‰ with $\Delta_n CaCO_3 \sim 0.1$, whereas Sites 738 and 690 have 4‰ excursions and $\Delta_n CaCO_3$ of 0.2 to 0.3. Similarly, at Site 1210 the bulk $CaCO_3$ CIE magnitude is 2.1‰ and $\Delta_n CaCO_3$ is ~0.1, but at Site 690 the bulk $CaCO_3$ CIE magnitude is 2.8‰ with $\Delta_n CaCO_3$ of 0.3. The excursion magnitudes do not appear to be a function of initial $CaCO_3$ wt% (Fig. 3-1B) or paleodepth (Fig. 3-1C).

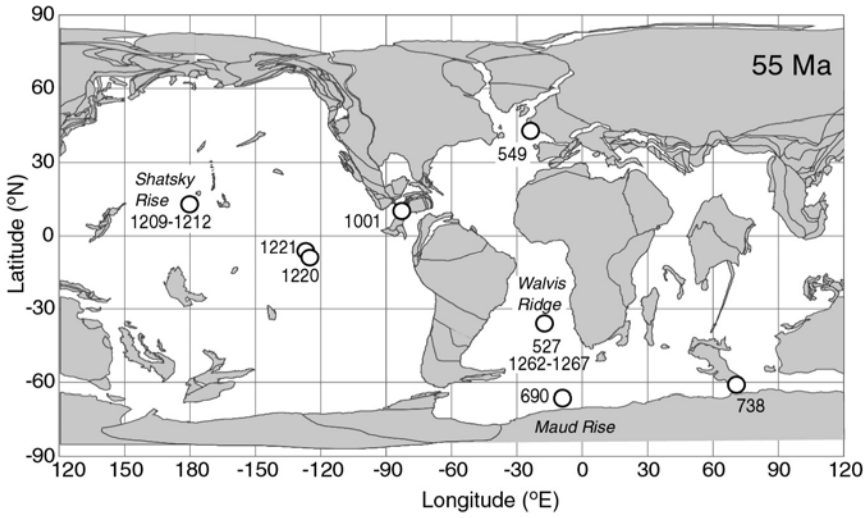

Figure 3-2: Late Paleocene paleogeography showing the location of sites in Fig. 3-1. Paleogeographic reconstruction by the Advanced Plate Reconstruction Service of the Ocean Drilling Stratigraphic Network, www.odsn.de.

The relationship between the magnitude of the CIE and $CaCO_3$ content in Fig. 3-1A does not rule out the possibility that $CaCO_3$ dissolution muted CIE records in deep sea sediments, but it does suggest that other factors may have played a role. Our objective in this paper is to determine what those factors might have been and to address the underlying question, which is broadly applicable to events throughout Earth history, "How much different is the $\delta^{13}C$ record preserved in sediments from the history of $\delta^{13}C$ in the seawater from which those sediments originated?"

Of course, this question is difficult to answer because we have no direct samples of ancient seawater with which to reconstruct the oceanic $\delta^{13}C$ history. Instead, we have approached the problem with a numerical Earth system model, GENIE-1, which allows us to analyze the propagation of a simulated PETM $\delta^{13}C$ signal in both seawater and preserved sediments. GENIE-1 has a 3D-ocean biogeochemistry model, as well as a sediment component that both simulates $CaCO_3$ preservation on the sea floor and generates a stratigraphic record as sediments accumulate. These model features allow us to compare the PETM $\delta^{13}C$ signal as it appears in surface ocean dissolved inorganic carbon (DIC) to its expression in newly produced $CaCO_3$, in core-top $CaCO_3$, and in the stratigraphic record.

Our previous use of GENIE-1 to study the PETM (Chapter 2) focused on calculating the spatial distribution of $CaCO_3$ wt% to provide a constraint on the source of C necessary to generate the presumed PETM $\delta^{13}C$ excursion. Here we extend that work to explore the relationship between actual and preserved carbon isotope excursions to both further constrain the sources and sizes of C inputs during the PETM, and more

generally assess the nature of the isotopic record of C-cycle variations in the geologic past.

We explore several factors that may have influenced the $\delta^{13}C$ excursion. These include the potential for fractionation-related damping of the excursion in newly produced $CaCO_3$, the effects of spatial variability in the pre-PETM $\delta^{13}C$ of surface ocean DIC ($\delta^{13}C_{DIC}$), the effects of dissolution of "old" $CaCO_3$ with relatively high $\delta^{13}C$ on the CIE, and the role of bioturbation. We find that the primary determinant of the CIE magnitude preserved in sediments is the delay between the onset of isotopic recovery of surface water DIC and the resumption of sedimentation at a particular model site.

Methods

The GENIE-1 Earth system model (Edwards and Marsh, 2005) is driven by a frictional geostrophic 3-D ocean circulation model (Edwards, 1996) coupled to a 2-D energy-moisture balance model (EMBM) of the atmosphere and a dynamic-thermodynamic sea-ice model based on that of Weaver et al. (2001). Also included is a marine carbon-cycle model (Ridgwell et al., 2007) and a model of biogenic carbonate sedimentation (Ridgwell and Hargreaves, 2007). Configuration of the model for the PETM is discussed in Chapter 2. Detailed descriptions of all components are available in the sources cited above, so here we focus on the model components of most interest to this investigation, those that deal with the production and preservation of $CaCO_3$ and isotopic changes in the carbon cycle. These components are illustrated schematically in Fig. 3-3.

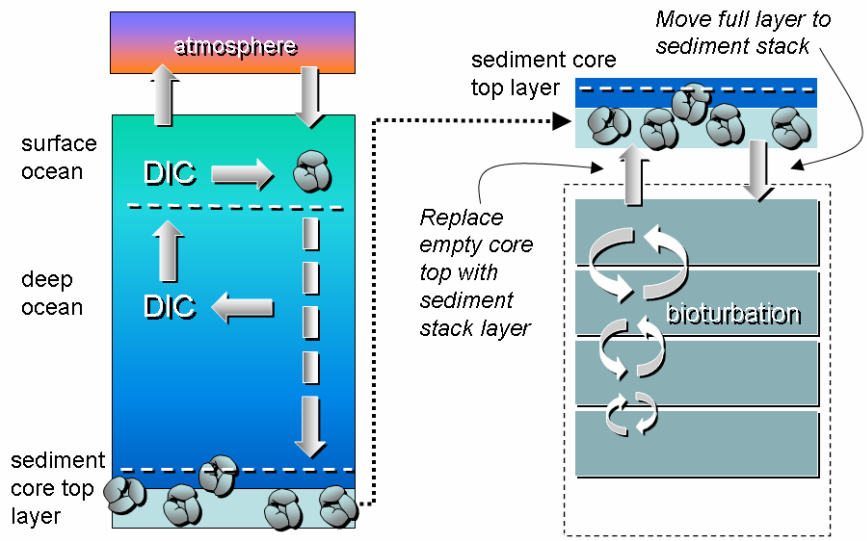

Figure 3-3: Schematic illustration of the GENIE-1 Earth system model. White arrows indicate transport directions. Forams ( ) symbolize newly produced $CaCO_3$ with $\delta^{13}C$ representative of the surface ocean.

In the model, production of new $CaCO_3$ in the surface ocean is ultimately determined by the PO_4^{3-} concentration in the surface layer. Particulate organic carbon (POC) export is calculated from the PO_4^{3-} concentration using a Monod growth formulation. Export of $CaCO_3$ is determined by a prescribed rain ratio (see Chapter 2), which sets the $CaCO_3$ export relative to the POC export. New $CaCO_3$ has $\delta^{13}C$ equal to that of surface ocean DIC plus a positive fractionation term that increases with temperature (after Mook, 1986). New $CaCO_3$ and POC fall through the water column and undergo dissolution according to an exponential function with length scales of 1055 m and 556 m, respectively (Ridgwell et al., 2007).

All POC reaching the sea floor is remineralized and returned to the water column, and the CO_2 evolved is available to dissolve $CaCO_3$ within the sediments. $CaCO_3$ reaching the sea floor is added to the core-top sediment layer with 1 cm maximum

thickness. If the core-top layer is full, it is moved down into a sediment stack, and accumulation on the sea floor continues until sediments in the core-top layer are once again 1 cm thick. If the sea floor sediment layer is emptied, as by dissolution, then the top sediment stack layer is moved up to take its place. In this way the model sediment core may have gaps if long periods of non-deposition occur, or if layers of the core are "unburied" and dissolved, similar to the "burn-down" thought to take place at the PETM (e.g., Zachos et al., 2005; Colosimo et al., 2006). Non-carbonate detrital material is accumulated along with $CaCO_3$ at 0.18 g cm^{-2} ka^{-1}. This rate was tuned to improve the model approximation of the pre-PETM $CaCO_3$ distribution, but it differs little from a value typical of the modern Pacific Ocean and one used in previous long-term fossil-fuel CO_2 removal simulations by Archer et al. (1998), 0.16 g cm^{-2} ka^{-1}. Without the non-carbonate detrital component, the $CaCO_3$ wt% could be only 0% or 100%.

Within the sediment stack, sediments can undergo bioturbation. Bioturbation is represented as mixing between adjacent sediment layers, where the mixing rate is a maximum of 16 cm^2 ka^{-1} in the top layer and decreases with an e-folding depth of 1 cm (Ridgwell, 2001). Bioturbation is important because it can bring $CaCO_3$ into the core-top layer as other $CaCO_3$ is dissolved and therefore increase the amount of $CaCO_3$ available to react with CO_2 in seawater. This ultimately increases the CO_2 uptake capacity of the ocean.

Although model time may be applied directly to DIC or core-top records, this does not work for the sediment stack because any one layer may contain sediments accumulated at different model times. This is accommodated by introducing an age tracer. The age tracer behaves as any other conservative tracer, and the age of a sediment

stack layer is the weighted average of the ages of sediments making it up, in the same way that the $\delta^{13}C$ of bulk carbonate represents the weighted average of $\delta^{13}C$ of its components.

The simulations shown here include three of the scenarios that have been suggested to explain the PETM: release of biogenic methane from methane clathrates ($\delta^{13}C$ of –60‰), oxidation of organic carbon ($\delta^{13}C$ of –22‰), and emission of mantle CO_2 by volcanism ($\delta^{13}C$ of –5‰). The size of the CO_2 pulse in each case is that which generates a -4‰ excursion in the combined ocean-atmosphere carbon reservoir. For the biogenic methane, organic carbon, and mantle CO_2 scenarios, the necessary pulse sizes are 2,300, 7,000, and 70,000 Pg C, respectively. Three additional simulations were run to fill the gap between the 7,000 and 70,000 Pg C pulses. These have $\delta^{13}C$ of -12, -9.5, and -6‰ and pulse sizes of 15,000, 21,000, and 46,000 Pg C, respectively. These scenarios can be viewed as some of the possible combinations of thermogenic methane ($\delta^{13}C$ of -35 to -50‰, Hunt, 1996) and volcanic (i.e., mantle-derived) CO_2 discharged into the atmosphere during North Atlantic Igneous Province (NAIP) volcanism (e.g., Svensen et al., 2004; Storey et al., 2007). Indeed, pulses with $\delta^{13}C$ of -22‰ and lower could also be consistent with carbon derived from NAIP volcanism.

The model was spun up for 150 ka with pCO_2 of 750 ppm and a flux of 50 Tmol HCO_3^- a^{-1} from rivers (see Chapter 2 for details) to achieve geochemical steady state and to build up a sufficient depth of sediments. After spin-up a pulse of carbon in the form of CO_2 was released to the atmosphere at a uniform rate over 10,000 years (after Dickens, 2003). At the end of 10,000 years the pulse was stopped and the model was run

for an additional 100,000 years. Each scenario was run with bioturbation, and the 2,300 and 7,000 Pg C scenarios were also run without bioturbation. Here we examine the sedimentary records produced by the model to understand how the record of $\delta^{13}C_{DIC}$ preserved in sediments might have been affected by dissolution.

Results

The response of the model climate to the ensemble of carbon-release scenarios is summarized in Fig. 3-4B,C: Atmospheric pCO_2 ranged between 1,140 (2,300 Pg C pulse) and 25,500 ppm (70,000 Pg C pulse) immediately after 10 ka of carbon addition (Fig 3-4B). At this time sea surface temperature (SST) was also at its peak, having warmed by 1.5°C to 14°C (Fig. 3-4C). A doubling of atmospheric pCO_2 (from 750 ppm to 1500 ppm) yielded 1°C of warming of the globally averaged SST (Fig. 3-4D).

There are several key features in the timeseries of $\delta^{13}C_{DIC}$, core-top layer $CaCO_3$ $\delta^{13}C$ ($\delta^{13}C_{CT}$), and core-top layer $CaCO_3$ wt% (Figs. 3-4E-G, respectively) that provide important clues about the factors affecting how the pulse of low $\delta^{13}C$ CO_2 to the atmosphere is eventually recorded in the sediments.

Surface ocean DIC $\delta^{13}C$

The larger the CO_2 pulse to the atmosphere, the smaller the $\delta^{13}C_{DIC}$ excursion (Fig. 3-4E). The CIE is the largest for the 2,300 Pg C case, at nearly -4‰, and the smallest for the 70,000 Pg C case, at ~-2‰. The decrease in CIE magnitude reflects a

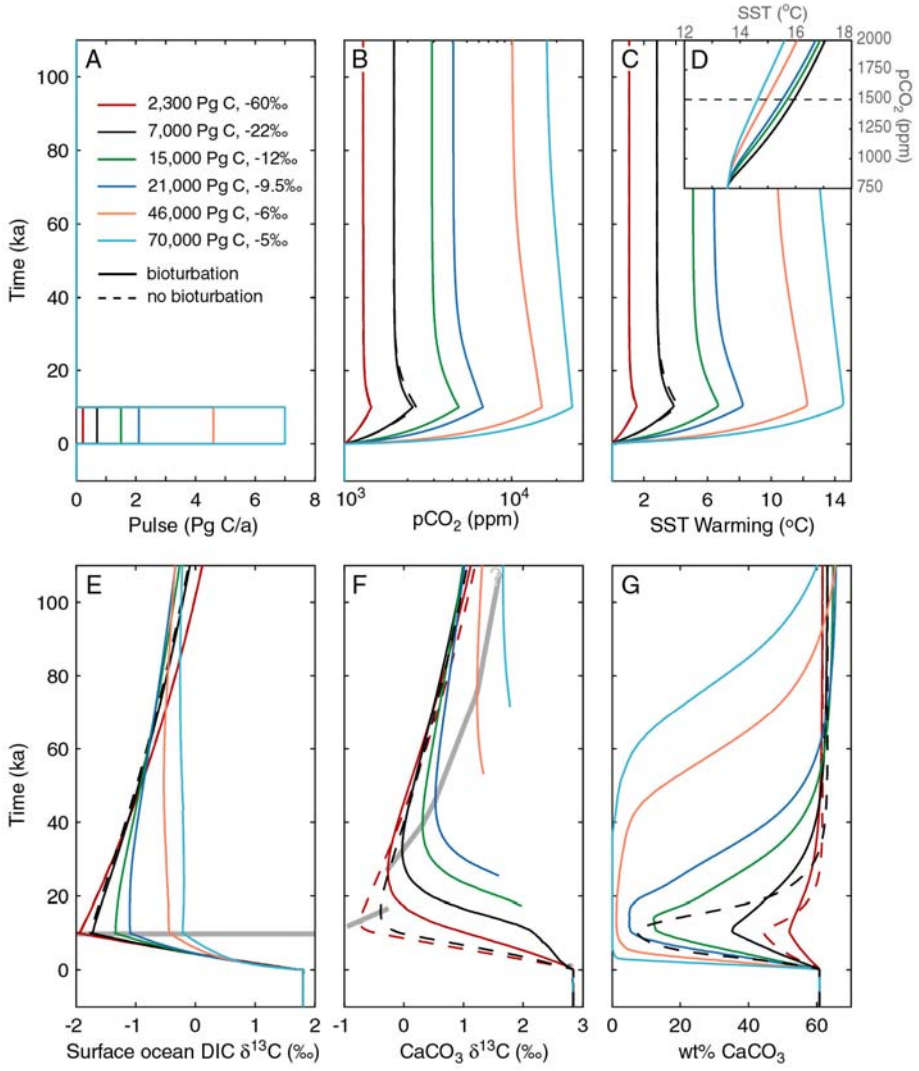

Figure 3-4: Globally averaged timeseries of system properties. A) low $\delta^{13}C$ pulse input signal; B) atmospheric pCO_2; C) increase in sea surface temperatures (SST); D) sensitivity of global average SST to increasing atmospheric CO_2 (dashed line marks pCO_2 doubling from the initial 750 ppm); E) $\delta^{13}C$ of surface ocean DIC (grey line indicates the peak of the excursion at 10 ka); F) $\delta^{13}C$ of $CaCO_3$ in sediment core-top layer (grey line intersects results at peak excursion); G) $CaCO_3$ content of sediment core-top layer.

decrease in the net burial of $CaCO_3$ as seawater saturation with respect to calcite (Ω) decreases, and eventually seawater becomes undersaturated ($\Omega<1$; $\Omega = 1$ indicates saturation, and $\Omega>1$ indicates supersaturation). The flux of carbon from rivers is no

longer balanced by the flux of carbon to the sediments. Furthermore, old $CaCO_3$, deposited prior to the onset of the PETM, is dissolved. Because the old $CaCO_3$ was produced from surface ocean DIC when $\delta^{13}C_{DIC}$ was higher, dissolution of old $CaCO_3$ contributes higher $\delta^{13}C$ carbon to the DIC pool, offsetting some of the isotopic effects of the low $\delta^{13}C$ carbon pulse. For the 2,300 Pg C cases, the system carbon reservoir is ~ 3,300 Pg C larger by the end of the 10 ka carbon pulse, indicating that ~ 1,000 Pg C was added to the system above the 2,300 Pg C pulse. For the 7,000 Pg C cases the system carbon reservoir is >2,000 Pg C larger than expected, and for the 70,000 Pg C case decreased net deposition accounts for a further 7,600 Pg C.

There is an additional level of complexity to the $\delta^{13}C_{DIC}$ response: for a given carbon-release scenario, DIC exhibits a range of $\delta^{13}C$ values, and the range is wider for larger carbon pulses (Fig. 3-5A). For the 2,300 Pg C cases, the range is ~ 0.5‰, and for the 70,000 Pg C case the range is nearly 2‰. The range varies smoothly with the initial $\delta^{13}C_{DIC}$ (Fig. 3-5B).

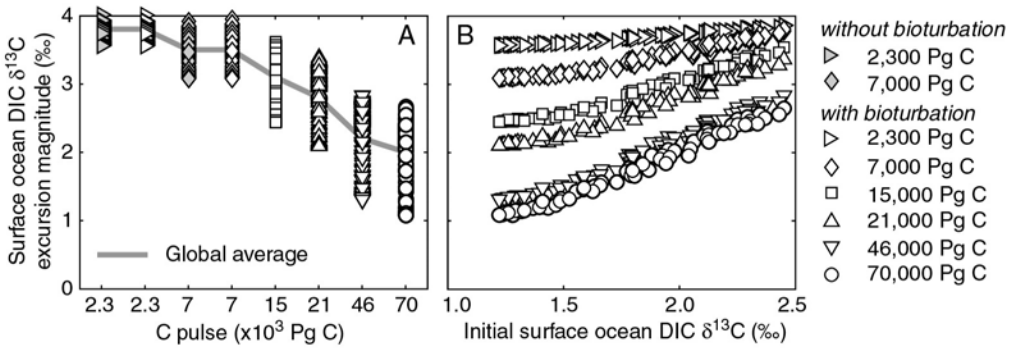

Figure 3-5: A) $\delta^{13}C_{DIC}$ CIE magnitudes of individual model sites for each carbon-release scenario. B) Relationship between the initial $\delta^{13}C_{DIC}$ and the $\delta^{13}C_{DIC}$ excursion magnitude, reflecting two-component mixing.

This relationship is an expected outcome of the two-component mixing taking place between the newly-added low-$\delta^{13}C$ CO_2 and surface ocean DIC. By re-arranging mass balance and isotope mass balance equations (Eqs. 3-2 and 3-3, respectively), where M is mass, δ is $\delta^{13}C$, and the subscripts i, a, and f refer to initial, added, and final quantities, respectively, we see that the $\delta^{13}C_{DIC}$ excursion ($\varepsilon = \delta_f - \delta_i$) is proportional to the difference between the $\delta^{13}C$ of the CO_2 pulse and the initial $\delta^{13}C_{DIC}$, and to the ratio of the mass of added carbon to the final (total) mass of carbon in the system:

$$M_f = M_i + M_a \qquad \text{(Eq. 3-2)}$$

$$\delta_f M_f = \delta_i M_i + \delta_a M_a \qquad \text{(Eq. 3-3)}$$

$$\varepsilon = (\delta_a - \delta_i)\frac{M_a}{M_f} \qquad \text{(Eq.3-4)}$$

The greater the difference in $\delta^{13}C$ between the initial reservoir and the added carbon, the larger the excursion magnitude will be. The larger the ratio of M_a to M_f, the greater the range of excursions. Consequently, the magnitude of the excursion due to biogenic methane is large because of the large difference between the $\delta^{13}C$ of methane (-60‰) and the $\delta^{13}C$ of surface ocean DIC (~-1 to -2‰), but the range of excursion magnitudes is small. On the other hand, the excursion caused by mantle CO_2 (-5‰) is much smaller, but the larger pulse size amplifies the effects of variations in the initial $\delta^{13}C_{DIC}$.

Core-top $CaCO_3$ record

Like the globally averaged $\delta^{13}C_{DIC}$, the magnitude of the CIE in $\delta^{13}C_{CT}$ also decreases for larger pulse sizes, but the magnitudes of $CaCO_3$ CIEs are smaller than those

of $\delta^{13}C_{DIC}$ (Fig. 3-4F). In general, the global average $\delta^{13}C_{DIC}$ is the upper bound of the range of CIE magnitudes in the core-top record (Fig. 3-6A).

Some of the difference between DIC and core top $CaCO_3$ excursion magnitudes can be accounted for by the increase in carbon isotopic fractionation between surface ocean DIC and newly produced $CaCO_3$. Initially, fractionation results in $CaCO_3$ $\delta^{13}C$ values of ~1‰ higher than the DIC from which the $CaCO_3$ is formed. As the temperature increases in response to the CO_2 pulse, the positive fractionation becomes larger, and the net increase in fractionation offsets the negative $\delta^{13}C$ excursion. The amount of damping by changes in fractionation (Fig. 3-6C) corresponds roughly to the difference between the $\delta^{13}C_{CT}$ and $\delta^{13}C_{DIC}$ excursions in the case of the three or four largest pulses, but for the smaller pulses it leaves most of the difference unaccounted for.

Another feature of the globally-averaged $\delta^{13}C_{CT}$ timeseries is that, whereas the peak of the CIE in the surface ocean occurs at the end of the 10 ka carbon pulse for all cases, the peak of the CIE in the core-top $CaCO_3$ is delayed, and the delay is longer for larger carbon pulses (heavy grey lines intersect the peak $\delta^{13}C$ values in Fig. 3-4F, cf. grey line in Fig. 3-4E). The time elapsed between the $\delta^{13}C_{DIC}$ peak and the $\delta^{13}C_{CT}$ peak (Δt_p and Δt_p' in Fig. 3-7A, where the prime indicates the presence of bioturbation) is due in part to a delay between the onset of the $\delta^{13}C_{DIC}$ (i.e., at the start of the carbon pulse) and the onset of the $\delta^{13}C_{CT}$ CIE (the intervals Δt_o and Δt_o' in Fig. 3-7A). The delay in the onset of the $\delta^{13}C_{CT}$ CIE reflects the interval after the pulse begins during which seawater becomes undersaturated with respect to calcite, so there is no net deposition of $CaCO_3$ (Δt_o and Δt_o' in Fig. 3-7B) and therefore no medium to record $\delta^{13}C_{DIC}$.

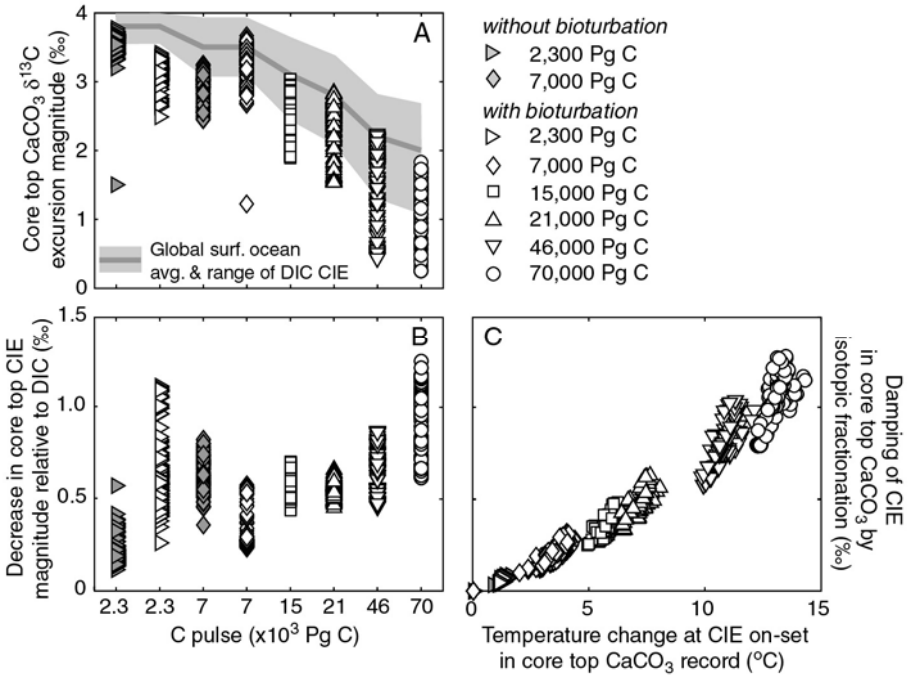

Figure 3-6: A) $\delta^{13}C_{CT}$ excursion magnitude for each carbon-release scenario. B) Damping of the $\delta^{13}C_{CT}$ CIE relative to the $\delta^{13}C_{DIC}$ CIE for each scenario. C) Damping of the $\delta^{13}C_{CT}$ CIE due to temperature-related changes in isotopic fractionation between DIC and $CaCO_3$.

For the case without bioturbation illustrated in Fig. 3-7, a small part of the beginning of the excursion is recorded while net sedimentation persists (i.e., while $\Omega>1$, up to *a* in Fig. 3-7A,B). When all available $CaCO_3$ is used up, the rate of dissolution is exactly equal to the rate of deposition, and the record of the excursion stops (*c* in Fig. 3-7B,C). Approximately 4 ka after the carbon pulse stops, seawater at this site is no longer undersaturated with respect to calcite. The rate of dissolution decreases below the rate of deposition, $CaCO_3$ begins to accumulate, and the record of $\delta^{13}C_{DIC}$ resumes, having missed the peak of the excursion.

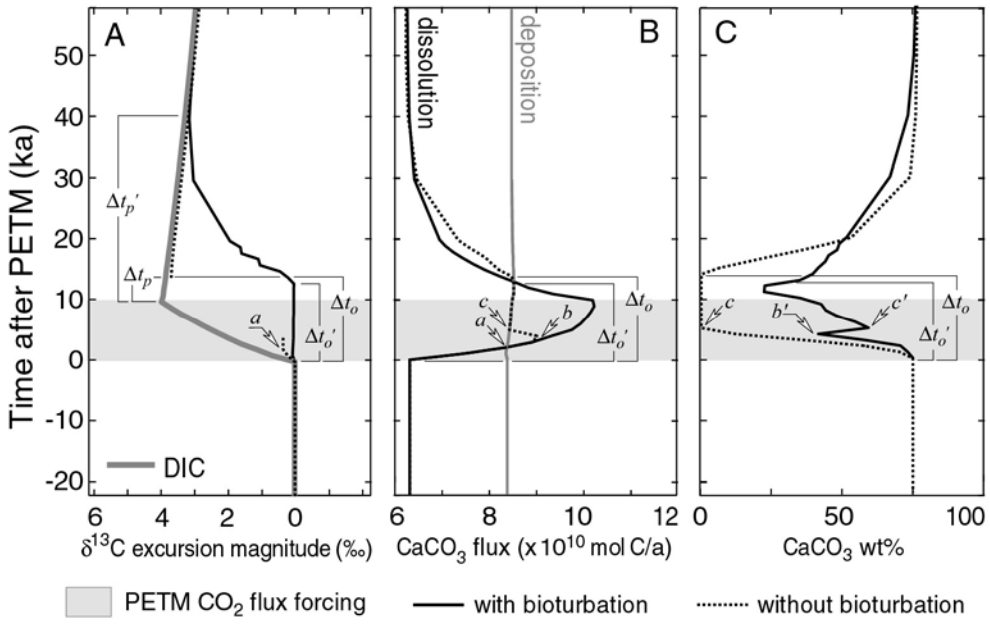

Figure 3-7**:** Model DIC and core-top timeseries for the 7,000 Pg C cases from Shatsky Rise. All points labelled with the same letter occur at the same time. Labels with primes indicate the case with bioturbation. The intervals Δt_p and $\Delta t_p'$ are the delays between the peak of the excursion in DIC and the peak of the excursion in the core-top record. The intervals Δt_o and $\Delta t_o'$ are the delays between the onset of the excursion in DIC and the onset of the excursion in the core-top record. A)$\delta^{13}C_{CT}$ excursion magnitude superimposed on the $\delta^{13}C_{DIC}$ record (heavy grey line). B) Rates of dissolution (black lines) and deposition (grey line; deposition is the same for bioturbated and non-bioturbated cases). C) Core-top $CaCO_3$ wt% timeseries.

When bioturbation is present, however, the timing of the peak is affected by the on-going supply of old $CaCO_3$ from the sediments in addition to the length of time required for recovery of Ω. At the onset of the pulse, the dissolution flux follows the same trajectory as before, until the point where the non-bioturbation scenario ran out of available $CaCO_3$ (Fig. 3-7B, *b*). Here the dissolution flux for the bioturbation case continues to increase until the pulse stops, because Ω is still decreasing as a result of CO_2 addition, and because bioturbation provides a ready supply of old $CaCO_3$ to be dissolved.

In this case, $CaCO_3$ wt% does not go to zero because dissolution is sufficiently slow compared to the resupply of old $CaCO_3$ by bioturbation. In fact, the difference in rates between these two processes results in double $CaCO_3$ wt% minima. The first minimum (Fig. 3-7C, *b'*) occurs when the old $CaCO_3$ immediately available in the surface layer is used up. Despite the fact that the rate of dissolution continues to rise in this case, there is a brief period during which the $CaCO_3$ wt% increases because the rate of bioturbation is supplying $CaCO_3$ in excess of the dissolution rate. When the dissolution rate increases beyond the sum of the supply rates of bioturbation and deposition (Fig. 3-7C, *c'*), $CaCO_3$ wt% falls again until shortly after the pulse stops.

When the rate of dissolution falls below the rate of accumulation, the $\delta^{13}C$ excursion appears in the core-top record. Until then, $\delta^{13}C_{CT}$ continues to reflect the $\delta^{13}C$ of old $CaCO_3$. The time elapsed between the onset of the $\delta^{13}C$ excursion in bioturbated sediments and its peak is a function of the rate of new $CaCO_3$ accumulation relative to the rate of mixing of new $CaCO_3$ with old. The excursion peaks and matches the $\delta^{13}C_{DIC}$ trajectory when enough new $CaCO_3$ has accumulated such that dilution by old, higher $\delta^{13}C$ $CaCO_3$ becomes negligible. The maximum possible $\delta^{13}C_{CT}$ excursion in either case is therefore dependent upon the rates of recovery of sedimentation and of $\delta^{13}C_{DIC}$.

It appears that the presence or absence of bioturbation has substantial consequences for the preservation of $CaCO_3$ in the sediments and on the $\delta^{13}C_{CT}$ profile. Where sediments are not bioturbated, $\delta^{13}C$ and $CaCO_3$ wt% decrease more rapidly. The $\delta^{13}C_{CT}$ CIE is larger and sharper in cases without bioturbation, and the global average $CaCO_3$ wt% is lower compared to sediments with bioturbation for the same pulse size

(Figs. 3-4G, 3-7C). Given the response of core-top $CaCO_3$ content, it is perhaps counterintuitive that *less* $CaCO_3$ is dissolved in the absence of bioturbation than when bioturbation is present. Without bioturbation, the $CaCO_3$ available for dissolution is limited by what is immediately available at the sediment surface. When this is depleted, a cap of non-carbonate detrital material remains and impedes interaction by diffusion with $CaCO_3$ deeper in the sediment column. In contrast, with bioturbation previously-buried $CaCO_3$ is moved back into the sediment surface layer and becomes available for dissolution. Consequently, the CO_2 uptake capacity of the ocean is reduced in the absence of bioturbation. For the 7,000 Pg C case without bioturbation, both pCO_2 and temperature are slightly higher than the case with bioturbation (Fig. 3-4B,C). This effect would be more pronounced for larger carbon pulses because the 7,000 Pg C case without bioturbation already comes close to dissolving most of the available $CaCO_3$ globally (see Fig. 2-4D), so more of the carbon from larger pulses would remain in the atmosphere.

Sediment-core $CaCO_3$ record

The difference between the core-top record and the sediment-core record is that the core top is an instantaneous snapshot of the sediment conditions on the sea floor, whereas the sediment core reflects the processes that occur after the surface layer becomes buried. This difference does not appear to affect the magnitude of the $\delta^{13}C$ excursion that is recorded; for the most part there is a one-to-one relationship between core top and sediment-core $\delta^{13}C$ excursion magnitudes (Fig. 3-8A).

The delay between the peak of the $\delta^{13}C_{DIC}$ excursion and the $\delta^{13}C$ excursion in $CaCO_3$ tends to be smaller in the sediment core than in the core top, except for the 70,000 Pg C case, and some model sites in the 46,000 Pg C case (Fig. 3-8B). Variability in delay times is also slightly less for the sediment core, although the delay times in the sediment cores tend to fall within the range of delay times for the core-top records. The delay in the core-top record depends in part on when net deposition resumes. This is also true for the sediment-core record, but the timing of the excursion can then be modified by bioturbation within the sediment stack; while bioturbation delays the peak of the excursion in the core-top record, it advances the peak in the sediment core relative to the core-top excursion, and advances the onset of the excursion so that it appears to begin

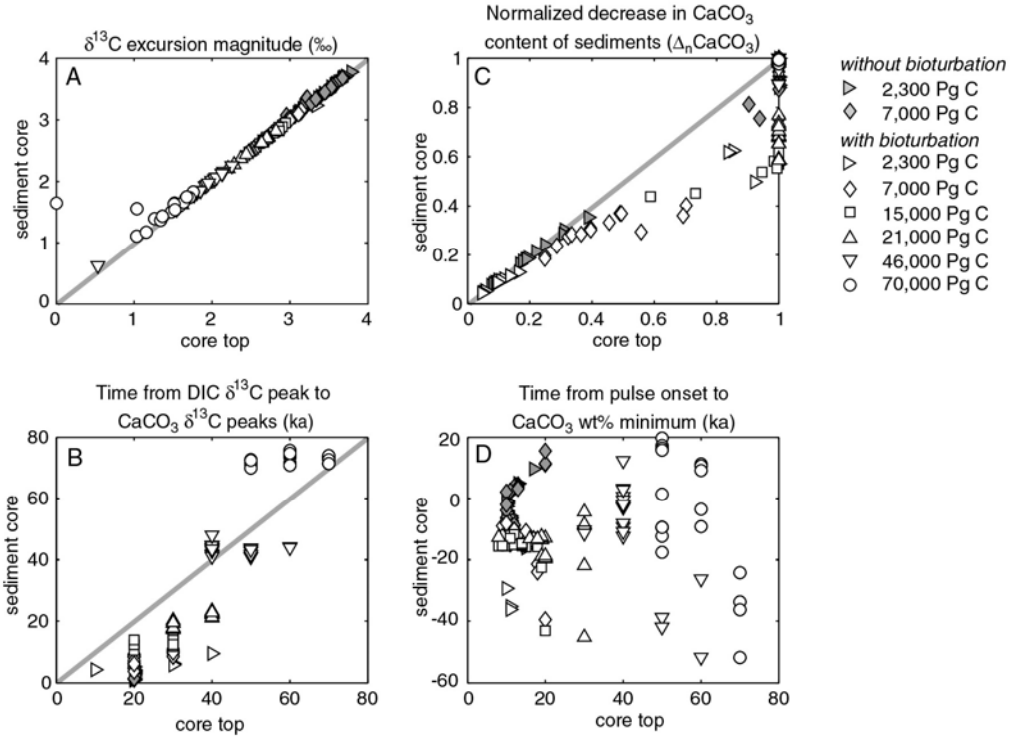

Figure 3-8: Comparison of core top and sediment-core records.

before the $\delta^{13}C_{DIC}$ excursion (Fig. 3-9A). This occurs because dissolution of $CaCO_3$ in sediments eventually results in new $CaCO_3$ being deposited on sediments older than the PETM, and bioturbation mixes the $\delta^{13}C$ of the new $CaCO_3$ downcore. In contrast, when bioturbation is not present, the magnitude and timing of the excursion in the core top and the sediment core are essentially the same (Fig. 3-9B).

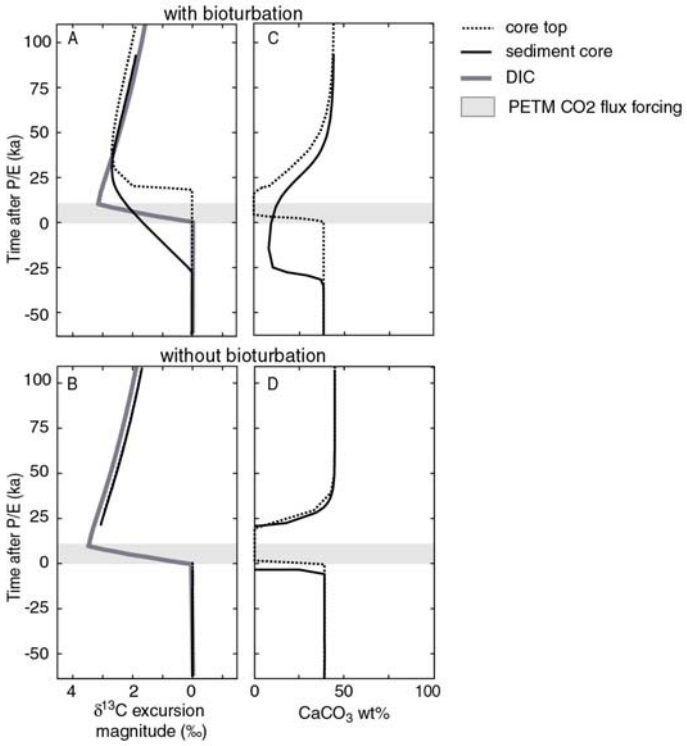

Figure 3-9: Comparison of core top and sediment-core $\delta^{13}C$ excursion and $CaCO_3$ wt% profiles from a 5000 m deep site at Walvis Ridge for the 7,000 Pg C cases with and without bioturbation.

The change in $CaCO_3$ wt% during the PETM is very similar for sediment core and core-top records when the decrease in $CaCO_3$ wt% is relatively small, but when larger fractions of $CaCO_3$ in sediment dissolves, there is less of a decrease in the sediment-core $CaCO_3$ content than in the core-top $CaCO_3$ content (Fig. 3-8C). This is also an effect of

bioturbation; even when the $CaCO_3$ wt% of the core-top record is zero, the sediment core may record a non-zero $CaCO_3$ wt% because bioturbation mixes carbonate-free sediments with older sediments still containing $CaCO_3$ (Fig. 3-9C). As with the $\delta^{13}C$ record, downcore mixing of carbonate-free sediment with older $CaCO_3$–rich sediment advances the onset of the $CaCO_3$ decline so that it appears to occur before the carbon pulse is added. Without bioturbation, 0 wt% $CaCO_3$ in the core top will be recorded as such in the sediment core (Fig 3-9D).

Comparison of observed and modeled CIE magnitudes

The CIE magnitudes observed in the data do not have a straightforward relationship with the decrease in $CaCO_3$ wt% (Fig. 3-1), and neither do the excursion magnitudes in the sediment core (Fig. 3-10). The 2,300 and 7,000 Pg C cases without bioturbation have the largest excursion magnitudes, ~3.5‰ on average; the 2,300 Pg C case spans a range of $\Delta_n CaCO_3$ from 0.1 to 1 (from a 10% decrease in $CaCO_3$ wt% to a 100% decrease) with no apparent change in CIE magnitude, and the 7,000 Pg C case plots in the range of $\Delta_n CaCO_3$ from 0.7 to 1. The 2,300 and 7,000 Pg C cases with bioturbation have average CIE magnitudes of ~3 ‰, and also cover a wide range of $\Delta_n CaCO_3$ without showing an obvious decrease in CIE magnitude when the decrease in $CaCO_3$ wt% is greater. The other cases tend toward higher values of $\Delta_n CaCO_3$ and lower CIE magnitudes as pulse sizes become larger, but they still display a considerable range of excursion magnitudes. For example, the 70,000 Pg C case has excursions between 0 and -2‰ despite having $\Delta_n CaCO_3$ of 1 or close to 1 in all cases.

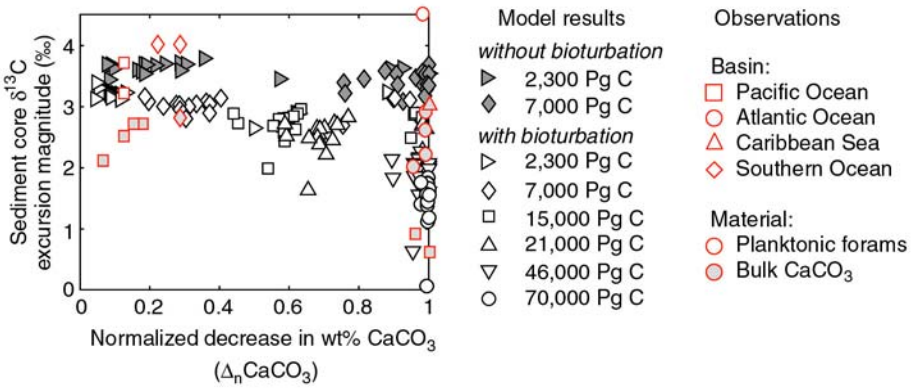

Figure 3-10: Comparison of $\delta^{13}C$ excursion magnitude vs. normalized decrease in wt% $CaCO_3$ between model sediment-core results and observations. See Appendix A and Table 3-1 for data and sources.

No single case modeled here is consistent with all of the observations. In the low $\Delta_n CaCO_3$ region of Fig. 3-10 (left-hand side) the Pacific ocean data from planktonic foraminifera fall within the range of results for the 2,300 Pg C cases with and without bioturbation, but the Southern Ocean planktonic foram observations have $\delta^{13}C$ excursions larger than any of the model results. Excursions recorded in bulk carbonate from the Pacific fall below the range of model results, although the bulk carbonate measurement from the Southern Ocean falls within the range of the 7,000 Pg C case with bioturbation. On the right hand side of the plot, all observations have $\Delta_n CaCO_3$ >0.9. The largest excursion is -4.5‰, from northern Atlantic Ocean planktonic forams, and well above the range of model results. The Caribbean Sea observation from bulk carbonate falls within the range of the 7,000 to 15,000 Pg C cases; the Atlantic Ocean (Walvis Ridge) bulk carbonate observations fall within the range of the 7,000 to 46,000 Pg C cases; and the two bulk carbonate measurements from the Pacific are within the range of the 46,000 to 70,000 Pg C cases.

Discussion

In this study pulses of CO_2 were added to the atmosphere in amounts calculated to decrease the $\delta^{13}C$ of the system carbon reservoir (ocean plus atmosphere) by 4‰. However, at each step toward recording the change in $\delta^{13}C$ in the sediments, there are factors at play that can modify the $\delta^{13}C$ signal: The $\delta^{13}C_{DIC}$ CIE magnitude depends on the initial $\delta^{13}C_{DIC}$, where a greater difference between the initial $\delta^{13}C_{DIC}$ and the $\delta^{13}C$ of the CO_2 pulse yields a larger excursion (Fig. 3-5, Eq. 3-4), and on the amount of old, relatively high $\delta^{13}C$ $CaCO_3$ that is dissolved as a result of the carbon pulse and added back into the ocean-atmosphere reservoir (Fig. 3-4E). The formation of $CaCO_3$ from DIC includes a temperature-dependent fractionation step that damps the CIE in new $CaCO_3$ compared to DIC (Fig. 3-6). The CIE magnitude is further decreased if there is a long period of undersaturation of seawater with respect to calcite. While $\Omega<1$, no new $CaCO_3$ accumulates, so there is no record of the $\delta^{13}C$ history in the surface ocean. When the perturbation to Ω is small, deposition recovers more rapidly and more of the $\delta^{13}C_{DIC}$ excursion is recorded. When the perturbation is large and deposition recovers later, the sediment record may miss much of the largest part of the excursion. In the presence of bioturbation, new $CaCO_3$ is diluted by old, and it is not until enough new $CaCO_3$ has accumulated to make dilution negligible that sediments will begin to reflect $\delta^{13}C_{DIC}$. Bioturbation can affect sediments long after they are buried. While this appears to have a negligible effect on the magnitude of the $\delta^{13}C$ excursion recorded in the sediment core, bioturbation mixes low $CaCO_3$ or $CaCO_3$-free sediments with sediments having higher $CaCO_3$ wt%. Consequently, a higher $CaCO_3$ wt% is recorded than may have existed.

Overall, this behavior does not result in a straightforward relationship between the magnitude of the $\delta^{13}C$ excursion and the gap in the sedimentary record as indicated by the normalized decrease in $CaCO_3$ wt% (Fig. 3-10), but it does suggest a framework for interpreting this relationship.

Our results predict that the largest excursions occur where the recovery time of Ω is shorter. As an indication of the degree of undersaturation, a site with more rapid recovery should be a site with less of a decrease in $CaCO_3$ wt% or, in terms of Fig. 3-10, lower $\Delta_n CaCO_3$. On the other hand, results predict larger excursions in the absence of bioturbation. Because bioturbation results in higher $CaCO_3$ wt% for a given pulse size than when bioturbation is not occurring, this implies that larger excursions should occur with higher $\Delta_n CaCO_3$. Therefore, the relationship between $CaCO_3$ content changes and the $\delta^{13}C$ excursion magnitude is unlikely to be a simple one for a suite of sites in which some are bioturbated, and some are not, or cease to be during the PETM event.

In this light, one way to view Figs. 3-1 and 3-10 is that they show two response regimes to the PETM carbon pulse: On the right hand side are sites for which the degree of perturbation of Ω is the main control on recovery time, and therefore on excursion magnitude. On the left are sites for which the rate of bioturbational mixing is the more important control on recovery time and excursion magnitude. Observations of lithologies of sites in Fig. 3-1 tend to support this scheme. On the right hand side, the sites for which we predict that recovery from undersaturation is the most important control include Walvis Ridge, for which bioturbation is reported to be nearly absent during the PETM at Site 1266 (Shipboard Scientific Party, 2004c), and absent for Sites 1262 and 1263

(Shipboard Scientific Party, 2004a, b). Diminished bioturbation is reported at Site 1001 for the PETM (Bralower et al., 1997). Laminae are present at Site 1220 during the PETM (Shipboard Scientific Party, 2002a). At Site 1221, bioturbation is present as burrows, and diminishes downcore within the PETM section (Shipboard Scientific Party, 2002b). In contrast, on the left hand side of Fig. 3-1, the Shatsky Rise sites and Site 690 display bioturbation throughout the PETM interval (Bralower et al., 1995; Thomas and Shackleton, 1996; Colosimo et al., 2006).

There is some support to be gained for this interpretation from the timescales of observed profiles of bulk carbonate $\delta^{13}C$ and $CaCO_3$ wt% from Walvis Ridge (Zachos et al., 2005). In Fig. 3-11, profiles are shown for Site 1262 (3600 m paleodepth), and Site 1263 (1500 m paleodepth) in blue. Model synthetic sediment cores (black lines) from depths of 3,600 m and 1,800 m in the Walvis Ridge region are superimposed. For Site 1262, the 2,300 Pg C scenario with bioturbation (Fig. 3-11A) comes the closest to matching the magnitude of the $\delta^{13}C$ excursion, but the onset and recovery of the excursion are much faster for the model sediment core than in the observed profile. The 21,000 and 46,000 Pg C cases come closer to matching the initial rate of the excursion, but do not produce an excursion of the appropriate magnitude (Fig. 3-11J,N). The 46,000 and 70,000 Pg C cases come closest to matching the $CaCO_3$ wt% profile at 1262 (Fig. 3-11P). For 1263, the shallower of the two sites, the 7,000 Pg C cases (Fig. 3-11G) come closest to matching the rate of the onset of the $\delta^{13}C$ excursion, but none of the model scenarios reproduces the excursion magnitude.

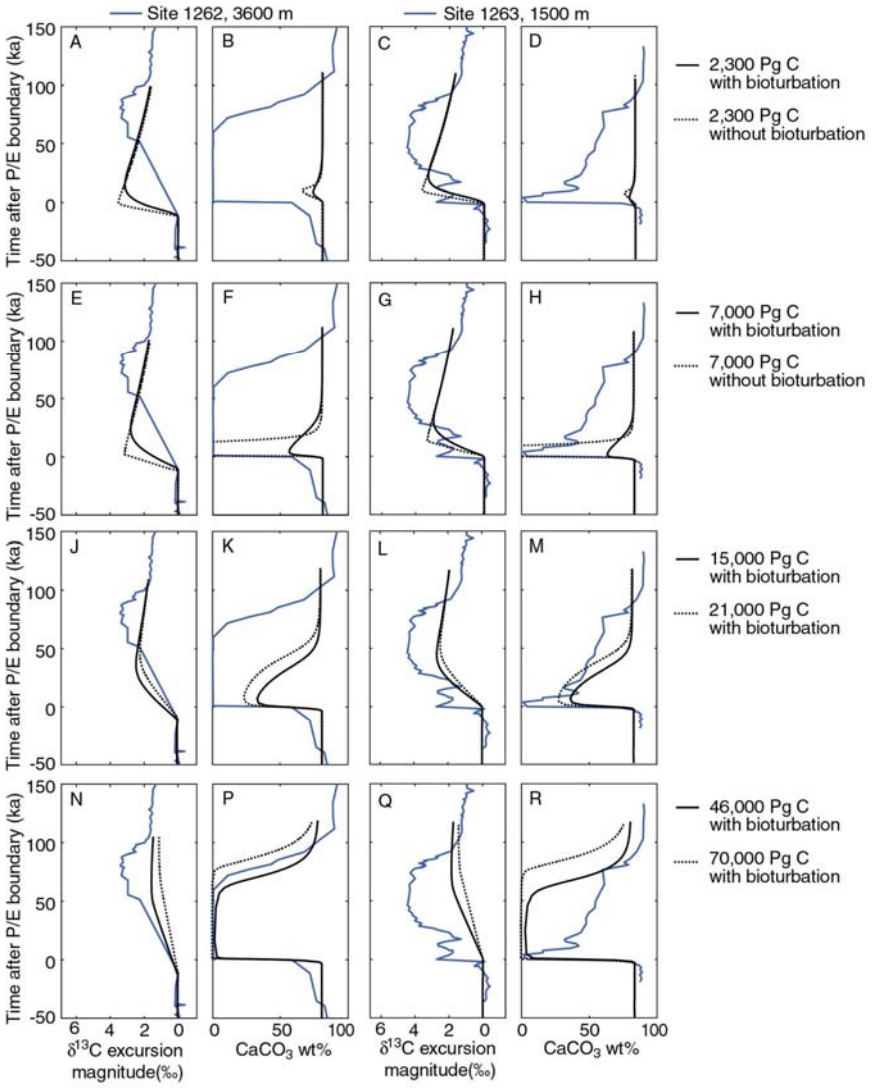

Figure 3-11: Comparison of sediment-core results with observations from Walvis Ridge by Zachos et al. (2005).

The 7,000 Pg C case without bioturbation (Fig. 3-11H) comes closest to reproducing the initial sharp decrease and recovery in the $CaCO_3$ wt% record, but no simulation reproduces the subsequent slower recovery. In summary, pulses of 21,000 Pg C and larger offer the better match to the $CaCO_3$ wt% record and to the rate of the $\delta^{13}C$

excursion for the deeper site, 1262, but do not generate a large enough $\delta^{13}C$ excursion; for the shallower site, 1263, the 7,000 Pg C scenarios appear to offer a better match to the initial drop and recovery of the $CaCO_3$ wt% record and to the rate of onset of the $\delta^{13}C$ excursion, but do not provide a large enough $\delta^{13}C$ excursion. Despite the apparent lack of a consistent answer about the appropriate pulse size on the part of the model, it is interesting to note that the scenarios with timescales that come closest to matching the timescales of the Walvis Ridge records are also the scenarios that plot in the same locations as Sites 1262 and 1263 in Fig. 3-10.

Overall, the model-data comparison in Fig. 3-11 does present some conflicting results. First, the best match to the Site 1262 $CaCO_3$ wt% record comes from model scenarios with bioturbation, but evidence cited above indicates that there was little to no bioturbation at Walvis Ridge during the PETM. One explanation is that bioturbation decreased or stopped altogether at the PETM, but by the time the Ω recovered to allow burial of $CaCO_3$, bioturbation had recovered. This idea was offered by Ridgwell (submitted) to explain the apparent change in $CaCO_3$ wt% recovery rates at Site 1263 and others at Walvis Ridge.

A second conflicting result is the pulse sizes suggested by the sites at Walvis Ridge. At Site 1263, the model-data comparison suggests that the 7,000 Pg C pulse comes very close to simulating the PETM record. At Site 1262, however, it appears that a pulse closer to 70,000 Pg C than 7,000 Pg C would be a better approximation of what happened at the PETM. This may simply reflect the expected top-down recovery of the CCD, although a slow-down of ocean circulation could also contribute to the slower rate of recovery at the deeper site.

The model results shown here do not provide a clear-cut answer regarding the PETM., but they are informative nonetheless. The persistent underprediction of the $\delta^{13}C$ excursion in planktonic foraminifera by our model suggest that the excursion at the PETM was larger than -4‰, consistent with the larger $\delta^{13}C$ excursion in the terrestrial record. The difference between the marine and terrestrial $\delta^{13}C$ excursion magnitudes may be due to the fact that the entire $\delta^{13}C$ excursion cannot be recorded in marine $CaCO_3$ due to undersaturation, but that the terrestrial record has no similar limitations. The terrestrial $\delta^{13}C$ record would, however, be affected by the dissolution of old $CaCO_3$ because the higher $\delta^{13}C$ carbon would eventually enter the atmosphere. Therefore, mass balance calculations performed using the excursion recorded in the terrestrial record would likely underestimate either the $\delta^{13}C$ or the size of the PETM carbon pulse.

The behaviours of model sediments for different pulse sizes and with and without bioturbation suggest that while the changes in $CaCO_3$ wt% or $\delta^{13}C$ at a particular site may not be reliable indicators of pulse size, the timescale of the response might be. It remains to test the sensitivity of model timescales to weathering feedbacks and to different rates of mixing within the sediments, but in general, the similar range of timescales at Walvis Ridge and in our results is promising. If the timescale at Site 1263 at Walvis Ridge were a good indicator that the pulse at the PETM was ~7,000 Pg C, and if the terrestrial $\delta^{13}C$ excursion were representative of the PETM excursion, then given a system $\delta^{13}C$ of 0.5‰, the pulse would have had $\delta^{13}C$ of -28 to -39‰, suggesting a thermogenic methane component.

Conclusion

The magnitude of the PETM $\delta^{13}C$ excursion has been key to estimates of the size of the carbon pulse added to the global carbon-cycle at the Paleocene-Eocene boundary. The magnitude of the excursion is uncertain, however. While marine carbonate sediments record $\delta^{13}C$ excursions of -3 to- 4‰ on average, $\delta^{13}C$ excursions recorded on land tend to be -5 to -7‰. There are several processes which occur after low $\delta^{13}C$ CO_2 mixes with surface ocean DIC and before $CaCO_3$ is preserved in the sediments that affect how well the original signal from DIC is propagated and preserved in the rock record. Our model results suggest that a particularly important consideration is the timescale of recovery of the saturation state of seawater with respect to calcite, where larger carbon pulses result in longer timescales. While seawater remains undersaturated, no net deposition of $CaCO_3$ occurs to record the $\delta^{13}C$ excursion in surface ocean DIC. The longer this condition persists, the further the $\delta^{13}C$ of DIC recovers toward pre-excursion values, and the smaller the excursion that will be recorded when $CaCO_3$ deposition resumes. Bioturbation is also a key factor, particularly when deposition resumes upon a low-$CaCO_3$ dissolution surface. By mixing older, higher $\delta^{13}C$ $CaCO_3$ with low $\delta^{13}C$ $CaCO_3$ deposited during the PETM, bioturbation results in a record that shows higher $\delta^{13}C$ values and higher $CaCO_3$ content than actually existed. The absence of similar "pause" and "rewind" mechanisms on land may explain the difference between terrestrial and marine PETM records.

We conclude, therefore, that the marine $\delta^{13}C$ excursion and the decrease in marine $CaCO_3$ wt% are not consistently reliable indicators of the amount of low $\delta^{13}C$ carbon

added to the Earth system to generate the PETM. The timescales of the system recovery as indicated by $\delta^{13}C$ and $CaCO_3$ wt% recovery in marine sediments might be informative, however. The shortest timescales could be used to place an upper bound on pulse size. The seemingly conflicting views of the size of the PETM pulse from the comparison of model sediment cores with $\delta^{13}C$ and $CaCO_3$ wt% data from Walvis Ridge likely stems in part from the expected top-down recovery of the CCD, which is a function of circulation patterns and weathering rates.

References

Archer, D., Kheshgi, H.S., and Maier-Reimer, E., 1998, Dynamics of fossil fuel CO_2 neutralization by marine $CaCO_3$: Global Biogeochemical Cycles, v. 12, p. 259-276.

Bains, S., Corfield, R.M., and Norris, R.D., 1999, Mechanisms of climate warming at the end of the Paleocene: Science, v. 285, p. 724-727.

Bowen, G.J., Beerling, D.J., Koch, P.L., Zachos, J.C., and Quattlebaum, T., 2004, A humid climate state during the Palaeocene/Eocene thermal maximum: Nature, v. 432, p. 495-499.

Bralower, T.J., Thomas, D.J., Zachos, J.C., Hirschmann, M.M., Rohl, U., Sigurdsson, H., Thomas, E., and Whitney, D.L., 1997, High-resolution records of the late Paleocene thermal maximum and circum-Caribbean volcanism: Is there a causal link?: Geology, v. 25, p. 963-966.

Bralower, T.J., Zachos, J.C., Thomas, E., Parrow, M., Paull, C.K., Kelly, C., Premoli Silva, I., Sliter, W.V., and Lohmann, K.C., 1995, Late Paleocene to Eocene paleoceanography of the equatorial Pacific Ocean: Stable isotopes recorded at Ocean Drilling Program Site 865, Allison Guyot: Paleoceanography, v. 10, p. 841-865.

Colosimo, A., Bralower, T.J., and Zachos, J.C., 2006, Evidence for lysocline shoaling at the Paleocene/Eocene Thermal Maximum on Shatsky Rise, Northwest Pacific, *in* Bralower, T.J., Premoli Silva, I., and Malone, M., eds., Proc. ODP., Sci. Results, 198: College Station, TX (Ocean Drilling Program), 1-36. doi:10.2973/odp.proc.sr.198.112.2006

Dickens, G.R., 2003, Rethinking the global carbon cycle with a large, dynamic and microbially mediated gas hydrate capacitor: Earth and Planetary Science Letters, p. 14.

Edwards, N.R., 1996, Unsteady similarity solutions and oscillating ocean gyres: Journal of Marine Research, v. 54, p. 793-826.

Edwards, N.R., and Marsh, R., 2005, Uncertainties due to transport-parameter sensitivity in an efficient 3-D ocean-climate model: Climate Dynamics, v. 24, p. 415-433.

Hunt, J.M., 1996, Petroleum geochemistry and geology: United States, W. H. Freeman and Company, New York, 743 p.

Lu, G., and Keller, G., 1993, The Paleocene-Eocene transition in the Antarctic Indian Ocean: Inference from planktonic foraminifera: Marine Micropaleontology, v. 21, p. 101-142.

Mook, W.G., 1986, ^{13}C in atmospheric CO_2: Netherlands Journal of Sea Research, v. 20, p. 211-223.

Nunes, F., and Norris, R.N., 2005, Data report: High-resolution stable isotope records across the Paleocene/ Eocene boundary, ODP Sites 1220 and 1221, *in* Wilson, P.A., Lyle, M., and Firth, J.V., eds., Proc. ODP, Sci. Results, 199, 1–12 [CD-ROM].

Pagani, M., Caldiera, K., Archer, D., and Zachos, J.C., 2006, An ancient carbon mystery: Science, v. 314, p. 1556-1557.

Pardo, A., Keller, G., Molina, E., and Canudo, J.I., 1997, Planktic foraminiferal turnover across the Paleocene-Eocene transition at DSDP Site 401, Bay of Biscay, North Atlantic: Marine Micropaleontology, v. 29, p. 129-158.

Ridgwell, A.J., 2001, Glacial-interglacial perturbations in the global carbon cycle [Ph.D. thesis], Univ. of East Anglia at Norwich, UK.

—, submitted, Marine sedimentary response to massive CO2 release: Implications for the interpretation of the PETM: Paleoceanography.

Ridgwell, A.J., and Hargreaves, J.C., 2007, Regulation of atmospheric CO_2 by deep-sea sediments in an Earth system model: Global Biogeochemical Cycles, v. 21, p. 14.

Ridgwell, A.J., Hargreaves, J.C., Edwards, N.R., Annan, J.D., Lenton, T.M., Yool, A., Marsh, R., and Watson, A.J., 2007, Marine geochemical data assimilation in an efficient Earth System Model of global biogeochemical cycling: Biogeosciences, v. 4, p. 87-104.

Shipboard Scientific Party, 2002a, Site 1220, *in* Lyle, M., Wilson, P.A., Janecek, T., et al., eds., Proc. ODP, Init. Repts., 199: College Station, TX (Ocean Drilling Program), 1-93. doi:10.2973/odp.proc.ir.199.113.2002

—, 2002b, Site 1221, *in* Lyle, M., Wilson, P.A., Janecek, T., et al., eds., Proc. ODP, Init. Repts., 199: College Station, TX (Ocean Drilling Program), 1-66. doi:10.2973/odp.proc.ir.199.114.2002

—, 2004a, Site 1262, *in* Zachos, J.C., Kroon, D., Blum, J.D., et al., eds., Proc. ODP, Init. Repts., 208: College Station, TX (Ocean Drilling Program), 1-92. 10.2973/odp.proc.ir.208.103.2004

—, 2004b, Site 1263, *in* Zachos, J.C., Kroon, D., Blum, J.D., et al., eds., Proc. ODP, Init. Repts., 208: College Station, TX (Ocean Drilling Program), 1-87. 10.2973/odp.proc.ir.208.104.2004

—, 2004c, Site 1266, *in* Zachos, J.C., Kroon, D., Blum, J.D., et al., eds., Proc. ODP, Init. Repts., 208: College Station, TX (Ocean Drilling Program), 1-79. 10.2973/odp.proc.ir.208.107.2004

Storey, M., Duncan, R.A., and Swisher, C.C.I., 2007, Paleocene-Eocene Thermal Maximum and the opening of the Northeast Atlantic: Science, v. 316, p. 587-589.

Stott, L.D., Sinha, A., Thiry, M., Aubry, M.-P., and Berggren, W.A., 1996, Global d13C changes across the Paleocene-Eocene boundary: criteria for terrestrial-marine correlations, *in* Knox, R.W.O.B., Corfield, R.M., and Dunay, R.E., eds., Correlation of the Early Paleogene in Northwest Europe, Geological Society Special Publication No. 101, p. 381-399.

Svensen, H., Planke, S., Malthe-Sorenssen, Jamtveit, B., Myklebust, R., Rasmussen Eidem, T., and Rey, S.S., 2004, Release of methane from a volcanic basin as a mechanism for initial Eocene global warming: Nature, v. 429, p. 542-545.

Thomas, D.J., Zachos, J.C., Bralower, T.J., Thomas, E., and Bohaty, S., 2002, Warming the fuel for the fire: Evidence for thermal dissociation of methane hydrate during the Paleocene-Eocene thermal maximum: Geology, v. 30, p. 1067-1070.

Thomas, E., and Shackleton, N.J., 1996, The Paleocene-Eocene benthic foraminiferal extinction and stable isotope anomalies, *in* Knox, R.W.O.B., Corfield, R.M., and Dunay, R.E., eds., Correlation of the Early Paleogene in Northwest Europe, Geological Society Special Publication No. 101, p. 401-441.

Weaver, A.J., Eby, M., Wiebe, E.C., Bitz, C.M., Duffy, P.B., Ewen, T.L., Fanning, A.F., Holland, M.M., MacFayden, A., Saenko, O., Schmittner, A., Wang, H., and Yoshimori, M., 2001, The UVic Earth System Climate Model: Model description, climatology, and applications to past, present, and future climates: Atmosphere-Ocean, v. 39, p. 68.

Zachos, J.C., Rohl, U., Schellenberg, S., Sluijs, A., Hodell, D.A., Kelly, D.C., Thomas, E., Nicolo, M., Raffi, I., Lourens, L.J., McCarren, H., and Kroon, D., 2005, Rapid acidification of the ocean during the Paleocene-Eocene Thermal Maximum: Science, v. 308, p. 1611-1615.

Zachos, J.C., Wara, M.W., Bohaty, S., Delaney, M.L., Petrizzo, M.R., Brill, A., Bralower, T.J., and Premoli Silva, I., 2003, A transient rise in tropical sea surface temperature during the Paleocene-Eocene Thermal Maximum: Science, v. 302, p. 1551-1554.

Appendix A

Paleodepth and $CaCO_3$ content data used in this study

Data plotted in Figs. 2-1B and 2-3 are listed under the appropriate sub-headings.

Site	Paleodepth		Sediment $CaCO_3$ wt%		
	Depth (m)	Source	Baseline	PETM	Source
Pacific Ocean					
164	5220	Van Andel (1975)	hiatus*	–	Van Andel (1975)
166	4880	Van Andel (1975)	hiatus*	–	Van Andel (1975)
170	5250	Van Andel (1975)	hiatus*	–	Van Andel (1975)
303	5540	Van Andel (1975)	hiatus*	–	Van Andel (1975)
304	5600	Van Andel (1975)	hiatus*	–	Van Andel (1975)
307	5520	Van Andel (1975)	hiatus*	–	Van Andel (1975)
313	3200	Van Andel (1975)	present	–	Van Andel (1975)
316	4020	Van Andel (1975)	hiatus*	–	Van Andel (1975)
1217	3200	Rea and Lyle (2005)	present	–	SSP (2002f)[§]
LL4-GPC3	–	–	absent	–	Kyte et al. (1993)
Shatsky Rise (a)					
577	1900	Miller et al. (1987)	96	hiatus	Bralower et al. (2002) Quillévéré et al. (2002)
1209	2000 – 2500	SSP (2002a)[§]	96	84	Colosimo et al. (2006)
1210	2000 – 3000	SSP (2002b)[§]	92	86	Colosimo et al. (2006)
1211	2000 – 3000	SSP (2002c)[§]	95	78	Colosimo et al. (2006)
1212	2000 – 3000	SSP (2002d)[§]	98	83	Colosimo et al. (2006)
Central Equatorial Pacific (b)					
163	4490	Van Andel (1975)	absent	–	Van Andel (1975)
165	4570	Van Andel (1975)	absent	–	Van Andel (1975)
315	4120	Van Andel (1975)	hiatus*	–	Van Andel (1975)
865	1300 – 1500	Thomas and Shackleton (1995)	96	93	Thomas et al. (1999) SSP (1995)[§]
1220	2900	Rea and Lyle (2005)	90	0	SSP (2002g)[§]
1221	3200	Rea and Lyle (2005)	74	3	Murphy et al. (2006)
168, 169	5000	Van Andel (1975)	hiatus*	–	Van Andel (1975)
Eastern Equatorial Pacific (c)					
1215	3200	Rea and Lyle (2005)	74	–	SSP (2002e)[§]
Caribbean Sea					
999	1750	Thomas et al. (1999)	61	0	Bralower et al. (1997)
1001	1500	Thomas et al. (1999)	45	0	Bralower et al. (1997)

This table is continues on the next page.

Table A: continued

Site	Paleodepth		Sediment $CaCO_3$ wt%		
	Depth (m)	Source	Baseline	PETM	Source
Atlantic Ocean					
527	3400	Moore et al. (1984)	83	0	Thomas et al. (1999)
549	2000 – 2300	Masson et al. (1985)	51	1	Thomas & Bralower (2005)
1050	–	–	63	57	Rudnicki et al. (2001)
1051	1000 - 2000	SSP(1998)[§]	56	52	Rudnicki et al. (2001)
Walvis Ridge (c)					
1262	3600	Zachos et al. (2005)	88	1	Zachos et al. (2005)
1263	1500	Zachos et al. (2005)	88	1	Zachos et al. (2005)
1266	2600	Zachos et al. (2005)	85	4	Zachos et al. (2005)
1267	3200	Inferred[†]	80	1	Zachos et al. (2005)
Southern Ocean, Atlantic sector (e)					
689	1400 – 1650	Kennett & Stott (1991)	91	–	SSP (1988)[§]
690	2100	Zachos et al. (1993)	84	60	Thomas et al. (1999)
Indian Ocean					
212	6050	Van Andel (1975)	hiatus*	–	Van Andel (1975)
215	3450	Van Andel (1975)	present	–	Van Andel (1975)
235	4300	Van Andel (1975)	absent	–	Van Andel (1975)
236	2740	Van Andel (1975)	present	–	Van Andel (1975)
240	3200	Van Andel (1975)	present	–	Van Andel (1975)
241	3990	Van Andel (1975)	absent	–	Van Andel (1975)
245	3560	Van Andel (1975)	present	–	Van Andel (1975)
250	5080	Van Andel (1975)	hiatus*	–	Van Andel (1975)
259	4430	Van Andel (1975)	present	–	Van Andel (1975)
260	5080	Van Andel (1975)	hiatus*	–	Van Andel (1975)
261	5400	Van Andel (1975)	hiatus*	–	Van Andel (1975)
Indian Ocean (f)					
211	4900	Van Andel (1975)	absent	–	Van Andel (1975)
213	3520	Van Andel (1975)	present	–	Van Andel (1975)
239	4220	Van Andel (1975)	absent	–	Van Andel (1975)
248	4170	Van Andel (1975)	hiatus*	–	Van Andel (1975)
256	5000	Van Andel (1975)	hiatus*	–	Van Andel (1975)
738	1350	Barrera & Huber (1991)	90	70	SSP (1989)[§]
766	3476	SSP (1990)[§]	93	–	SSP (1990)[§]
1135	1000 – 2000	Inferred[‡]	95	–	SSP (2000)[§]
1138	600 – 1200	Quilty (2002)**	93	–	SSP (2000)[§]

* Due to non-deposition

§ SSP = Shipboard Scientific Party

† At present, Site 1262 is 400 m deeper than 1267. To estimate a paleodepth for 1267, 400 m was subtracted from the paleodepth of Site 1262.

‡ Inferred from paleodepths of surrounding sites, including the Paleocene paleodepths of Sites 738 (Barerra and Huber, 1991), 747, and 748 (Mackensen and Berggren, 1992), and Late Maastrichtian paleodepths of Sites 747, 748, 750 (Quilty, 1992), and 1138 (Quilty, 2002), and given the bathymetric divisions of Berggren and Miller (1989).

** Late Campanian to Late Maastrichtian paleodepth.

References

Barrera, E., and Huber, B.T., 1991, Paleogene and Early Neogene oceanography of the Southern Indian Ocean: Leg 119 Foraminifer stable isotope results, in Barron, J., Larsen, B., Baldauf, J.G., et al., eds., Proc. ODP., Sci. Results, 119: College Station, TX (Ocean Drilling Program), 693 - 717

Berggren, W.A., and Miller, K.G., 1989, Cenozoic bathyal and abyssal calcareous benthic foraminiferal zonation: Micropaleontology, v. 35, p. 308-320.

Bralower, T.J., 2002, Evidence of surface water oligotrophy durign the Paleocene-Eocene thermal maximum: Nannofossil assemblage data from Ocean Drilling Program Site 690, Maud Rise, Weddell Sea: Paleoceanography, v. 17.

Bralower, T.J., Thomas, D.J., Zachos, J.C., Hirschmann, M.M., Rohl, U., Sigurdsson, H., Thomas, E., and Whitney, D.L., 1997, High-resolution records of the late Paleocene thermal maximum and circum-Caribbean volcanism: Is there a causal link?: Geology, v. 25, p. 963-966.

Colosimo, A., Bralower, T.J., and Zachos, J.C., 2006, Evidence for lysocline shoaling at the Paleocene/Eocene Thermal Maximum on Shatsky Rise, Northwest Pacific, in Bralower, T.J., Premoli Silva, I., and Malone, M., eds., Proc. ODP., Sci. Results, 198: College Station, TX (Ocean Drilling Program), 1-36. doi:10.2973/odp.proc.sr.198.112.2006

Kennett, J.P., and Stott, L.D., 1991, Abrupt deep-sea warming, palaeoceanographic changes and benthic extinctions at the end of the Paleocene: Nature, v. 353, p. 225-229.

Kyte, F.T., Leinen, M., Heath, R., and Zhou, L., 1993, Cenozoic sedimentation history of central North Pacific: Inferences from the elemental geochemistry of core LL44-GPC3: Geochimica et Cosmochimica Acta, v. 57, p. 1719-1740.

Mackensen, A., and Berggren, W.A., 1992, Paleogene benthic foraminifers from the southern Indian Ocean (Kerguelen Plateau); biostratigraphy and paleoecology, in Wise, S.W.J., Schlich, R., Julson, P., et al., eds., Proc. ODP, Sci. Results, 120: College Station, TX (Ocean Drilling Program), 603-630. doi:10.2973.odp.proc.sr.120.168.1992

Masson, D.G., Montandert, L., and Scrutton, R.A., 1985, Regional geology of the Goban Spur continental margin, in De Graciansky, P.C., Poag, C.W., Cunningham, R.J., et al., eds., Init. Repts. DSDP, 80: College Station, TX (Ocean Drilling Program), 1115-1139.

Miller, K.G., Janecek, T., Katz, M.E., and Keil, D.J., 1987, Abyssal circulation and benthic foraminiferal changes near the Paleocene/Eocene boundary: Paleoceanography, v. 2, p. 741-761.

Moore, T.C.J., Rabinowitz, P.D., Borella, P.E., Shackleton, N.J., and Boersma, A., 1984, History of the Walvis Ridge, in Moore, T.C.J., Rabinowitz, P.D., Boersma, A., et al., eds., Init. Repts. DSDP, 74: College Station, TX (Ocean Drilling Program), 873-894.

Murphy, B., Lyle, M., and Olivarez Lyle, A., 2006, Biogenic burial across the Paleocene/ Eocene boundary: Ocean Drilling Program Leg 199 Site 1221, in Wilson, P.A.,

Lyle, M., and Firth, J.V., eds., Proc. ODP., Sci.Results, 199: College Station, TX (Ocean Drilling Program), 1-12. doi:10.2973/odp.proc.sr.199.215.2006

Quillévéré, F., Aubry, M.-P., Norris, R.N., and Berggren, W.A., 2002, Paleocene oceanography of the eastern subtropical Indian Ocean: An integrated magnetobiostratigraphic and stable isotope study of ODP Hole 761B (Wombat Plateau): Palaeogeography, Palaeoclimatology, Palaeoecology, v. 184, p. 371-405.

Quilty, P., 1992, Upper Cretaceous benthic foraminifers and paleoenvironments, southern Kerguelen Plateau, Indian Ocean, in Wise, S.W.J., Schlich, R., Julson, P., et al., eds., Proc. ODP, Sci. Results, 120: College Station, TX (Ocean Drilling Program), 393-441. doi:10.2973.odp.proc.sr.120.173.1992

—, 2002, Paleoenvironmental significance of Late Cretaceous foraminifers from ODP Site 1138 samples, a dredge and Eltanin core E54-7, Kerguelen Plateau, Indian Ocean, in Quilty, P.G., ed., Proc. ODP, Sci. Results, 183: College Station, TX (Ocean Drilling Program), 1-28. doi:10.2973/odp.proc.sr.183.003.2002

Rea, D.K., and Lyle, M., 2005, Paleogene calcite compensation depth in the eastern subtropical Pacific: Answers and questions: Paleoceanography, v. 20, p. 9.

Shipboard Scientific Party, 1988, Site 689, *in* Barker, P.F., Kennett, J.P., O'Connell, S., et al., eds., Proc. ODP., Init. Repts., 113: College Station, TX (Ocean Drilling Program), 89-181. doi:10.2973/odp.proc.ir.113.106.1988

—, 1989, Site 738, *in* Barron, J., Larsen, B., Baldauf, J.G. et al., eds., Proc. ODP., Init. Repts., 119: College Station, TX (Ocean Drilling Program), 229-288

—, 1990, Site 766, in Gradstein, F.M., Ludden, J.N., Adamson, A.C., et al., eds., Proc. ODP., Init. Repts., 123: College Station, TX (Ocean Drilling Program), 269-352

—, 1995, Site 865, in Sinton, J.M., ed., Proc. ODP., Init. Repts., 143: College Station, TX (Ocean Drilling Program), 111-180. doi:10.2973/odp.proc.ir.143.106.1993

—, 1998, Site 1051, in Norris, R.D., Kroon, D., Klaus, A., et al., eds., Proc. ODP, Init. Repts., 171B: College Station, TX (Ocean Drilling Program), 171-239

—, 2000a, Site 1135, in Coffin, M.F., Frey, F.A., Wallace, P.J., et al., eds., Proc. ODP., Init. Repts., 183: College Station, TX (Ocean Drilling Program), 1-59. doi:10.2973/odp.proc.ir.183.103.2000

—, 2000b, Site 1138, in Coffin, M.F., Frey, F.A., Wallace, P.J., et al., eds., Proc. ODP., Init. Repts., 183: College Station, TX (Ocean Drilling Program), 1-213. doi:10.2973/odp.proc.ir.183.106.2000

—, 2002a, Site 1209, in Bralower, T.J., Premoli Silva, I., Malone, M., et al., eds., Proc. ODP, Init. Repts., 198: College Station, TX (Ocean Drilling Program), 1-102. doi:10.2973/odp.proc.ir.198.105.2002

—, 2002b, Site 1210, in Bralower, T.J., Premoli Silva, I., Malone, M., et al., eds., Proc. ODP, Init. Repts., 198: College Station, TX (Ocean Drilling Program), 1-89. doi:10.2973/odp.proc.ir.198.106.2002

—, 2002c, Site 1211, in Bralower, T.J., Premoli Silva, I., Malone, M., et al., eds., Proc. ODP, Init. Repts., 198: College Station, TX (Ocean Drilling Program), 1-81. doi:10.2973/odp.proc.ir.198.107.2002

—, 2002d, Site 1212, in Bralower, T.J., Premoli Silva, I., Malone, M., et al., eds., Proc. ODP, Init. Repts., 198: College Station, TX (Ocean Drilling Program), 1-79. doi:10.2973/odp.proc.ir.198.108.2002

—, 2002e, Site 1215, in Lyle, M., Wilson, P.A., Janecek, T., et al., eds., Proc. ODP, Init. Repts., 199: College Station, TX (Ocean Drilling Program), 1-60. doi:10.2973/odp.proc.ir.199.108.2002

—, 2002f, Site 1217, in Lyle, M., Wilson, P.A., Janecek, T., et al., eds., Proc. ODP, Init. Repts., 199: College Station, TX (Ocean Drilling Program), 1-60. doi:10.2973/odp.proc.ir.199.110.2002

—, 2002g, Site 1220, in Lyle, M., Wilson, P.A., Janecek, T., et al., eds., Proc. ODP, Init. Repts., 199: College Station, TX (Ocean Drilling Program), 1-66. doi:10.2973/odp.proc.ir.199.113.2002

Thomas, D.J., and Bralower, T.J., 2005, Sedimentary trace element constraints on the role of North Atlantic Igneous Province volcanism in late Paleocene - early Eocene environmental change: Marine Geology, v. 217, p. 233-254.

Thomas, D.J., Bralower, T.J., and Zachos, J.C., 1999, New evidence for subtropical warming during the late Paleocene thermal maximum: Stable isotopes from Deep Sea Drilling Project Site 527, Walvis Ridge: Paleoceanography, v. 14, p. 561-570.

Thomas, E., and Shackleton, N.J., 1996, The Paleocene-Eocene benthic foraminiferal extinction and stable isotope anomalies, in Knox, R.W.O.B., Corfield, R.M., and Dunay, R.E., eds., Correlation of the Early Paleogene in Northwest Europe, Geological Society Special Publication No. 101, p. 401-441.

Van Andel, T.H., 1975, Mesozoic/ Cenozoic calcite compensation depth and the global distribution of calcareous sediments: Earth and Planetary Science Letters, v. 26, p. 187-194.

Zachos, J.C., Lohmann, K.C., Walker, J.C.G., and Wise, S.W.J., 1993, Abrupt climate change and transient climates during the Paleogene: A marine perspective: Journal of Geology, v. 101, p. 191-213.

Zachos, J.C., Rohl, U., Schellenberg, S., Sluijs, A., Hodell, D.A., Kelly, D.C., Thomas, E., Nicolo, M., Raffi, I., Lourens, L.J., McCarren, H., and Kroon, D., 2005, Rapid acidification of the ocean during the Paleocene-Eocene Thermal Maximum: Science, v. 308, p. 1611-1615.

Appendix B

Model configuration

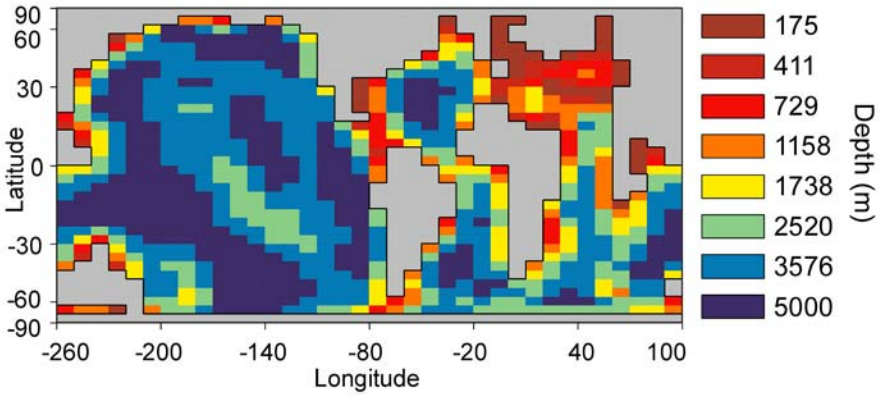

Figure B-1: Early Eocene bathymetry

Appendix C

Evaluation of goodness-of-fit between model output and observations

We address uncertainty regarding the Late Paleocene global weathering rate and the ratio of $CaCO_3$ to particulate organic carbon in the export of biogenic detritus from the surface ocean (the $CaCO_3$:POC rain ratio) by performing a 2-parameter sensitivity analysis comprising an ensemble of simulations with weathering fluxes of 30, 50, and 70 Tmol a^{-1} of HCO_3^- and spatiotemporally uniform rain ratios of 0.100, 0.175, and 0.250 Each ensemble member was spun up for 150 ka to reach geochemical equilibrium between weathering and sedimentation. The model $CaCO_3$ wt% output for each run is plotted in map view in Fig. C-1 with observations (sources listed in Appendix A) superimposed.

The best fit between model output and observed $CaCO_3$ wt% was identified by determining the lowest root mean squared error (RMSE) between model output and observations,

$$RMSE = \sqrt{\frac{1}{n}\Sigma(result - observation)^2} \qquad \text{Eq. C-1}$$

where n is the number of comparisons. First, $CaCO_3$ wt% was plotted versus depth for each of the model outcomes and the observations for three relatively data-rich regions: the central equatorial Pacific, Walvis Ridge in the Atlantic Ocean, and the southern Indian Ocean (identified as a, b, and c in Fig. 2-1A in the text). The profiles were fit using a linear weighted regression scheme described by Cleveland and Devlin (1988),

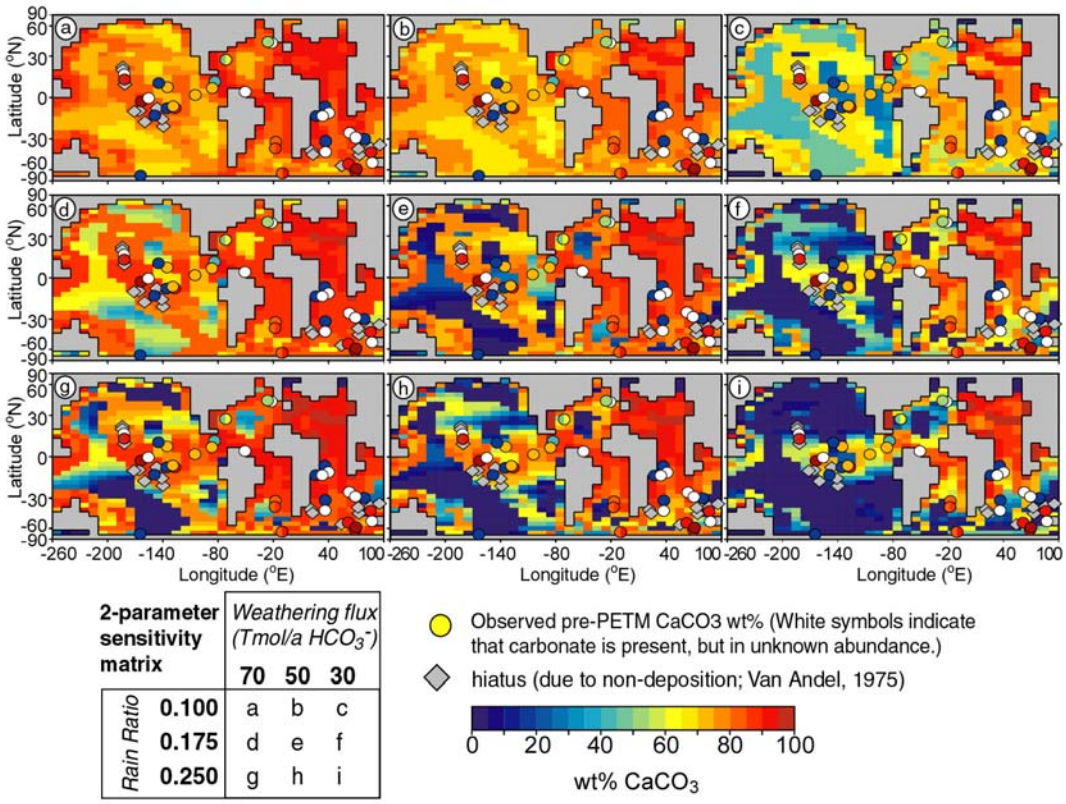

Figure C-1: Coretop $CaCO_3$ wt% output (maps) for an ensemble of model runs (panel labels correspond to the table in the legend) with observations superimposed (circle and diamond markers).

and available on-line in a data visualization toolbox (version 1.1) from Datatool (www.datatool.com) as the script loess.m for Matlab. This script requires that the user specify a set of points at which to compute the value of the fitted function, here set at 200 m increments; a smoothing parameter, α; and the order of the polynomial to be used by the Matlab function polyfit, λ. Values of α and λ are listed in Table C-1.

Next, the calculated fits to both model output and observations were evaluated at model layer depths encompassed by the paleodepths of observations. The RMSE was calculated for each region (Fig. C-2 A,B,C) and the total RMSE was computed (Fig. C-2D).

Table C-1: Parameters for loess.m

Case to fit	Smoothing (α)	Polynomial order (λ)
Observations		
central equatorial Pacific Ocean		
Initial	0.5	2
PETM	0.65	2
Walvis Ridge, southern Atlantic Ocean		
Initial	1	1
PETM	1	1
southern Indian Ocean		
Initial	0.75	1
Model results		
Initial conditions		
50 Tmol HCO_3^- a^{-1}, $CaCO_3$:POC of 0.175 and 0.250 in the southern Indian Ocean	0.75	1
70 Tmol HCO_3^- a^{-1}, $CaCO_3$:POC of 0.175 in the southern Indian Ocean	1	2
All other ensemble members and basins	1	1
PETM conditions	1	1

The best overall model-data fit (i.e., the scenario with the lowest total RMSE) is obtained with a $CaCO_3$:POC rain ratio of 0.175, higher than the mean value of ~0.14 characterizing the modern ocean (Ridgwell et al., 2007), and a total global weathering rate of 50 Tmol/a of HCO_3^-, which is larger than the 23-39 Tmol/a of HCO_3^- estimated for the modern (Munhoven, 2002) but less than that from early Eocene model simulations (Gibbs et al., 1999). The best overall model-data fit has a global average $CaCO_3$ wt% of 61%.

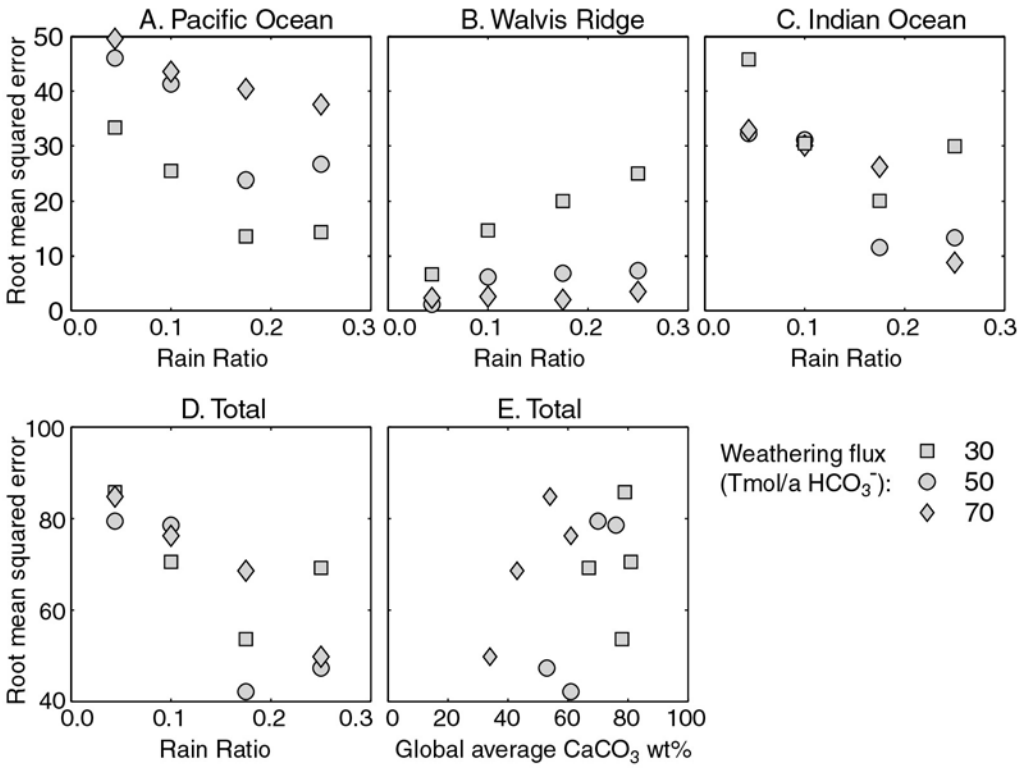

Figure C-2: Root mean squared errors (RMSE) for the 2-parameter sensitivity ensemble. The lowest overall RMSE (D, the sum of RMSE for data rich regions in A, B, and C) is achieved with a weathering flux of 50 Tmol/a of HCO_3^- and a rain ratio of 0.175. This scenario corresponds to a global average model $CaCO_3$ wt% of 61% (E).

The same analysis was performed to evaluate the best fit to observed PETM $CaCO_3$ wt% distributions (Fig. 2-6), except that the southern Indian Ocean region was not included because there are insufficient observations to generate a meaningful fit.

References

Cleveland, W.S., and Devlin, S.J., 1988, Locally Weighted Regression: An Approach to Regression Analysis by Local Fitting: Journal of the American Statistical Association, v. 83, p. 596-610.

Gibbs, M.T., Bluth, G.J.S., Fawcett, P.J., and Kump, L.R., 1999, Global chemical erosion over the last 250 My: variations due to changes in paleogeography, paleoclimate, and paleogeology: American Journal of Science, v. 299, p. 611-651.

Munhoven, G., 2002, Glacial–interglacial changes of continental weathering: estimates of the related CO_2 and HCO_3^- f lux variations and their uncertainties: Global and Planetary Change, v. 33, p. 155-176.

Ridgwell, A.J., Hargreaves, J.C., Edwards, N.R., Annan, J.D., Lenton, T.M., Yool, A., Marsh, R., and Watson, A.J., 2007, Marine geochemical data assimilation in an efficient Earth System Model of global biogeochemical cycling: Biogeosciences, v. 4, p. 87-104.

VITA

Karla Michelle Panchuk

Education

2007 **Doctor of Philosophy**, Department of Geosciences
Pennsylvania State University, University Park, Pennsylvania, United States

2002 **Master of Science**, Department of Geological Sciences
University of Saskatchewan, Saskatoon, Saskatchewan, Canada

1999 **Bachelor of Science with Honours**, Department of Geological Sciences
University of Saskatchewan, Saskatoon, Saskatchewan, Canada

Publications

Panchuk, K. M., Holmden, C. E., and Leslie, S. A. (2006) Local controls on carbon cycling in the Ordovician Midcontinent region of North America with implications for carbon isotope secular curves, *Journal of Sedimentary Research,* **76**, 10.2110/jsr.2006.017.

Panchuk, K. M., Holmden, C. E., and Kump, L. R. (2005) Sensitivity of the epeiric sea carbon isotope record to local-scale carbon cycle processes: Tales from the Mohawkian Sea, *Palaeogeography, Palaeoclimatology, Palaeoecology,* **228** (3-4), p. 320 – 337.